

Lucky spectroscopy, an equivalent technique to Lucky Imaging:

II. Spatially-resolved intermediate-resolution blue-violet spectroscopy of 19 close massive binaries using the William Herschel Telescope.

J. Maíz Apellániz¹, R. H. Barbá², C. Fariña^{3,4}, A. Sota⁵, M. Pantaleoni González^{1,6}, G. Holgado¹, I. Negueruela⁷, and S. Simón-Díaz^{3,8}

¹ Centro de Astrobiología, CSIC-INTA. Campus ESAC. Camino bajo del castillo s/n. E-28 692 Vill. de la Cañada. Madrid. Spain. e-mail: jmaiz@cab.inta-csic.es

² Departamento de Astronomía. Universidad de La Serena. Av. Cisternas 1200 Norte. La Serena. Chile.

³ Instituto de Astrofísica de Canarias. E-38 200 La Laguna, Tenerife. Spain.

⁴ Isaac Newton Group of Telescopes. Apartado de correos 321. E-38 700 Santa Cruz de La Palma, La Palma, Spain.

⁵ Instituto de Astrofísica de Andalucía-CSIC. Glorieta de la Astronomía s/n. E-18 008 Granada. Spain.

⁶ Departamento de Astrofísica y Física de la Atmósfera. Universidad Complutense de Madrid. E-28 040 Madrid. Spain.

⁷ Departamento de Física. Ingeniería de Sistemas y Teoría de la Señal. Escuela Politécnica Superior. Universidad de Alicante. Carretera San Vicente del Raspeig s/n. E-3690 San Vicente del Raspeig. Alicante. Spain.

⁸ Departamento de Astrofísica. Universidad de La Laguna. E-38 205 La Laguna, Tenerife. Spain.

Submitted 21 Sep 2020; accepted 23 Nov 2020

ABSTRACT

Context. Many massive stars have nearby companions whose presence hamper their characterization through spectroscopy.

Aims. We want to continue obtaining spatially resolved spectroscopy of close massive visual binaries to derive their spectral types.

Methods. We have used the lucky spectroscopy technique to obtain a large number of short long-slit spectroscopic exposures of 19 close visual binaries under good seeing conditions. We selected those with the best characteristics, extracted the spectra using multiple-profile fitting, and combined the results to derive spatially separated spectra. The results are analyzed in combination with data from lucky imaging, regular intermediate-resolution single-order spectroscopy, and échelle high-resolution spectroscopy.

Results. The new application of lucky spectroscopy has allowed us (among other results) to [a] spatially disentangle for the first time two O stars (FN CMa B and 6 Cas B) with brighter BA supergiant companions; [b] determine that two B stars (α Sco B and HD 164 492 B) with close and more massive companions are fast rotators (in the second case solving a case of mistaken identity); [c] extend the technique to cases with extreme magnitude differences (the previous two cases plus CS Cam A,B), shorter separations (HD 193 443 A,B), and fainter primary magnitudes down to $B = 11$ (HD 219 460 A,B); [d] spatially disentangle the spectra of stars with companions as diverse as an A supergiant (6 Cas A), a WR star (HD 219 460 B = WR 157), and an M supergiant (α Sco A); [e] discover the unexpected identity of some targets such as two previously unknown bright O stars (HD 51 756 B and BD +60 544) and a new member of the rare OC category (HD 8768 A); and [f] identify and classify (in some cases for the first time) which of the components of four visual binaries (σ Ori, HD 219 460, HD 194 649, and HD 191 201) is a double-lined spectroscopic binary while for another seven systems (FN CMa, σ Sco, HD 51 756, HD 218 195, HD 17 520, HD 24 431, and HD 164 492) we detect signs of spectroscopic binarity using high-spectral-resolution spectroscopy. We also present a determination of the limits of the technique.

Key words. binaries: spectroscopic — binaries: visual — methods: data analysis — stars: early-type — stars: massive — techniques: spectroscopic

1. Introduction

Massive stars are born in company of others but their multiplicity is not always easy to detect or characterize. The main complication lies in the large range of periods, from ~ 1 d orbits to systems that get to complete just one or a few revolutions during the lifetimes of the stars. Therefore, for a complete account of massive-star multiplicity one needs to use different techniques, as long-period systems are better studied by high-spatial-resolution techniques and short-period systems by high-spectral-resolution techniques. Putting it in a slightly different manner, the first type are usually studied as “visual binaries” (or multiples) and the second type as “spectroscopic binaries” (or multiples) (Mason et al. 1998) and in multiplicity studies it should be clear which type (one, the other, or both) we are refer-

ring to. Otherwise, confusion is likely to arise and wrong results will be obtained.

The first golden era of spectroscopic surveys of OB stars lasted from the 1950s to the 1970s. Morgan et al. (1955); Hiltner (1956); Lesh (1968); Hiltner et al. (1969); Walborn (1972, 1973); Garrison et al. (1977) are probably the best exponent of the results of that period. Interest in such surveys waned in the following two decades (with some exceptions) but regained strength in the 2000s with new technology and telescopes that significantly increased observing efficiency and with the need to address scientific issues such as the ubiquitous multiplicity already mentioned. As part of that renewed interest, for some time now we have been conducting different types of surveys that have the ultimate goal of characterizing massive stars and, more specifically, their multiplicity. With the Galactic O-

Table 1. Multiple systems observed with lucky spectroscopy in this paper. PC and SC refer to the primary and secondary visual components, respectively, and B_p is the B -band magnitude of the primary. For each observation we give the evening date, detector used (EEV for EEV12, QUC for QUCAM3), number of total exposures, number of exposures used for lucky spectroscopy (single value for EEV12, range for QUCAM3), exposure time (for one exposure), separation d (measured from the data), position angle used for the slit (which may be different from the one for the system), and magnitude difference in B (measured from the data).

Name	PC	SC	WDS ID	B_p	Even. date (YYMMDD)	Det.	n_{exp}	n_{used}	t_{exp} (s)	d ($''$)	PA ($^\circ$)	ΔB (mag)
FN CMa	A	B	J07067–1118	5.8	190220	EEV	120	60	1.00	0.57	109	1.2
					190917	EEV	100	15	1.00	0.57	109	1.2
6 Cas	A	B	J23488+6213	6.3	180729	EEV	143	65	1.00	1.50	194	2.3
α Sco	A	B	J16294–2626	2.8	120708	EEV	15	15	4.33	2.57	297	0.0
					180730	EEV	100	23	1.00	2.70	273	3.6
σ Sco	Aa	Ab	J16212–2536	3.2	180730	EEV	100	13	1.00	0.47	242	2.1
CS Cam	A	B	J03291+5956	4.6	190917	EEV	100	66	1.00	2.30	159	4.2
σ Ori	Aa,Ab	B	J05387–0236	4.4	170907	EEV	100	7	1.00	0.26	84	1.2
					181203	EEV	100	12	1.00	0.25	67	1.2
					190917	EEV	100	10	1.00	0.26	84	1.2
HD 5005	A	B	J00528+5638	8.6	181219	QUC	1004	100-402	1.00	1.53	82	1.6
					190906	EEV	100	58	1.00	1.53	82	1.6
HD 51 756	A	B	J06585–0301	7.8	181219	QUC	1004	26-51	1.00	0.63	100	0.3
HD 218 195	A	B	J23052+5815	8.7	181220	QUC	502	216-365	1.00	0.94	81	2.7
HD 219 460	A	B	J23152+6027	11.0	181220	QUC	502	423-499	1.00	1.38	127	0.3
HD 8768	A	B	J01281+6317	9.3	181220	QUC	502	138-247	1.00	0.66	28	2.8
BD +60 544	A	B	J02411+6108	10.4	181220	QUC	502	403-502	1.00	1.91	170	0.8
HD 17 520	A	B	J02512+6023	10.3	181220	QUC	502	262-279	1.00	0.32	298	0.7
HD 24 431	A	B	J03556+5238	7.2	181220	QUC	502	209-273	1.00	0.72	177	2.9
HD 164 492	A	B	J18024–2302	7.6	190914	EEV	100	71	1.00	6.19	20	3.6
HD 168 021	A	B	J18187–1837	7.4	190421	EEV	100	33	1.00	0.48	137	1.0
HD 193 443	A	B	J20189+3817	8.3	190731	EEV	100	13	1.00	0.14	258	0.3
HD 194 649	A	B	J20254+4014	10.6	190914	EEV	100	95	1.00	0.30	214	0.7
HD 191 201	A	B	J20074+3543	7.8	190914	EEV	100	47	1.00	1.00	84	1.8

Star Spectroscopic Survey (GOSSS, Maíz Apellániz et al. 2011) we are identifying and producing spectral classifications for O stars (and other massive stars) in the Galactic neighborhood with intermediate-resolution blue-violet spectroscopy. GOSSS has resulted in three major papers: Sota et al. 2011 (GOSSS I), Sota et al. 2014 (GOSSS II), and Maíz Apellániz et al. 2016 (GOSSS III), with a fourth paper in the series to be submitted soon. We have also collected a library of high-resolution spectroscopy of massive stars (LiLiMaRlin, Maíz Apellániz et al. 2019a) from public and private observations. In the northern hemisphere we are using it to study the spectroscopic multiplicity of O stars (MONOS project) of which the first paper appeared as Maíz Apellániz et al. 2019b (MONOS I) and a second paper will be submitted soon. In a parallel effort, GOSSS is also serving as a source of information for IACOB (Simón-Díaz et al. 2015b), a long-term project aimed at extending further the empirical characterization of Galactic O (and B) stars using quantitative high-resolution spectroscopy (see, e.g. Simón-Díaz et al. 2014, 2017; Holgado et al. 2018, 2020). As for high-spatial-resolution observations, we have observed a large number of systems with lucky imaging using AstraLux (Maíz Apellániz 2010 and MONOS I).

The surveys in the previous paragraph use either spectroscopic or high-spatial-resolution techniques but do not combine both. Therefore, in some cases such as hierarchical systems composed of a short-period spectroscopic binary and a close visual companion, it may not be clear how the three stars involved are related to each other or even what the precise spectral types of each may be (for an example, σ Ori, see Simón-Díaz et al. 2015a

and section 3.6). Combining both types of techniques (i.e. spectroscopy with high spatial resolution) addresses this issue. We have done this on the one hand using STIS spectroscopy with HST (Maíz Apellániz & Barbá 2020, from now on STIS I) or applying the novel technique of lucky spectroscopy (Maíz Apellániz et al. 2018, from now on LS I), which we developed in LS I. Lucky spectroscopy is the extension of lucky imaging (Law et al. 2006) to spectroscopy: we obtain a large number of short long-slit spectroscopic exposures under good-seeing conditions, select those with the best characteristics, and combine them to derive spatially resolved spectra of two or more closely separated point sources aligned with the slit.

In this paper we continue our analysis of massive close binaries with lucky spectroscopy that we started in LS I. In the next section we describe the main data in the paper, our new lucky spectroscopy observations for 19 close visual multiple systems, and their relationship with the previous data. We also describe there the complementary data we use to analyze those systems in the form of lucky imaging and other spectroscopy. In section 3 we present the results for our sample. We end up with a summary of our results and a brief presentation of our future plans.

2. Data and methods

2.1. Lucky spectroscopy

In LS I we presented lucky spectroscopy results for five bright (primaries with B magnitudes of 2-4) close visual binaries whose primaries have spectral subtypes between O7 and B0.7.

Table 2. Spectral classifications. GOS/GBS/GAS/GWS/GLS stand for Galactic O/B/A/WR/Late Star, respectively. The information in this table is also available in electronic form at the GOSC web site (<http://gosc.cab.inta-csic.es>).

Name	GOSSS ID	R.A. (J2000)	Decl. (J2000)	ST	LC	Qual.	Second.	Notes
FN CMa A	GBS 224.71–01.79_01	07:06:40.767	–11:17:38.46	B0.7	Ib	SB1 in LiLiMaRlin
FN CMa B	GOS 224.71–01.79_02	07:06:40.803	–11:17:38.71	O6	V	((f))z
6 Cas A	GAS 115.71+00.22_02	23:48:50.166	+62:12:52.22	A3	Ia
6 Cas B	GOS 115.71+00.22_01	23:48:50.108	+62:12:50.75	O9.5	II
α Sco A	GLS 351.95+15.06_01	16:29:24.461	–26:25:55.21	M1.5	Iab
α Sco B	GBS 351.95+15.06_02	16:29:24.275	–26:25:55.04	B2	V	n
σ Sco Aa	GBS 351.31+17.00_01	16:21:11.313	–25:35:34.09	B1	III	SB2 in LiLiMaRlin
σ Sco Ab	GBS 351.31+17.00_02	16:21:11.282	–25:35:34.30	B1:	V
CS Cam A	GBS 141.50+02.88_01	03:29:04.136	+59:56:25.20	B9	Ia
CS Cam B	GBS 141.50+02.88_02	03:29:04.252	+59:56:22.88	B2	III
σ Ori Aa,Ab	GOS 206.82–17.34_01	05:38:44.765	–02:36:00.25	O9.5	V	...	B0.2 V	In LS I + MONOS I
σ Ori B	GBS 206.82–17.34_02	05:38:44.782	–02:36:00.27	B0.2	V	(n)	...	In LS I + MONOS I
HD 5005 A	GOS 123.12–06.24_01	00:52:49.206	+56:37:39.49	O4.5	V	((fc))z	...	In GOSSS I
HD 5005 B	GBS 123.12–06.24_03	00:52:49.390	+56:37:39.71	B0	V	In GOSSS I
HD 51 756 A	GBS 216.42+00.18_01	06:58:28.180	–03:01:25.44	B0	IV	SB1? in LiLiMaRlin
HD 51 756 B	GOS 216.42+00.18_02	06:58:28.221	–03:01:25.57	O9.7	IV	(n)
HD 218 195 A	GOS 109.32–01.79_01	23:05:12.928	+58:14:29.34	O8.5	III	Nstr	...	In GOSSS I + II
HD 218 195 B	GBS 109.32–01.79_02	23:05:13.043	+58:14:29.49	B1.5	V	SB2? in LiLiMaRlin
HD 219 460 A	GBS 111.33–00.24_01	23:15:12.394	+60:27:01.84	B0.7	II	...	B1: III:	...
WR 157	GWS 111.33–00.24_02	23:15:12.542	+60:27:01.00	WN5
HD 8768 A	GOS 127.03+00.70_01	01:28:03.153	+63:16:57.20	OC9.2	II
HD 8768 B	GBS 127.03+00.70_02	01:28:03.198	+63:16:57.78	B0.7:	V
BD +60 544 A	GOS 135.78+01.03_01	02:41:08.194	+61:08:07.02	O9.5	IV
BD +60 544 B	GBS 135.78+01.03_02	02:41:08.244	+61:08:05.14	B1	V
HD 17 520 A	GOS 137.22+00.88_01	02:51:14.434	+60:23:09.97	O9.2	V	e	...	In GOSSS III
HD 17 520 B	GOS 137.22+00.88_02	02:51:14.396	+60:23:10.12	O8	V	z	...	In GOSSS III
HD 24 431 A	GOS 148.84–00.71_01	03:55:38.420	+52:38:28.75	O9	III	In GOSSS I
HD 24 431 B	GBS 148.84–00.71_02	03:55:38.424	+52:38:28.03	B1.5	V	SB1 in LiLiMaRlin
HD 164 492 A	GOS 007.00–00.25_01	18:02:23.553	–23:01:51.06	O7.5	V	z	...	In GOSSS II
HD 164 492 B	GBS 007.00–00.25_03	18:02:23.701	–23:01:45.14	B2	V	mn
HD 164 492 C	GBS 007.00–00.25_02	18:02:23.132	–23:02:00.17	B1	V	SB3 in LiLiMaRlin
HD 168 021 A	GBS 012.70–01.47_01	18:18:43.260	–18:37:10.81	B0	Ia
HD 168 021 B	GBS 012.70–01.47_02	18:18:43.281	–18:37:11.18	B0.2	II
HD 168 021 C	GBS 012.71–01.47_01	18:18:44.204	–18:36:59.94	B0.5	II
HD 193 443 A	GOS 076.15+01.28_01	20:18:51.707	+38:16:46.50	O8.5	III:	((f))	...	In MONOS I
HD 193 443 B	GOS 076.15+01.28_02	20:18:51.697	+38:16:46.48	O8.5	III	((f))	...	Sp. cl. from STIS I
HD 194 649 A	GOS 078.46+01.35_01	20:25:22.124	+40:13:01.07	O9.2:	IV:	In MONOS I
HD 194 649 B	GOS 078.46+01.35_02	20:25:22.109	+40:13:00.82	O9.2	IV	Sp. cl. from STIS I
HD 191 201 A	GOS 072.75+01.78_01	20:07:23.684	+35:43:05.91	O5.5	V	((f))	O9.5 V	In MONOS I
HD 191 201 B	GOS 072.75+01.78_02	20:07:23.766	+35:43:06.01	O7	V	z	...	In MONOS I
HD 191 201 C	GOS 072.75+01.78_03	20:07:23.766	+35:43:06.01	O9.5	III	...	B0 V	In MONOS I
HD 191 201 D	GOS 072.75+01.78_04	20:07:23.766	+35:43:06.01	O9.7	V	In MONOS I

The original data were obtained in September 2017 (though several tests had been previously performed, see below for an example) with the ISIS spectrograph at the William Herschel Telescope (WHT) and the success of the technique prompted us to attempt the separation of additional systems in 2018 and 2019. We had also obtained time for further observations in 2020 but those did not finally take place due to scheduling changes at WHT. Besides the obvious scientific interest of studying more objects for the knowledge of the members of the larger sample, there were several avenues we were interested in exploring:

- Repeatability of the results, including new epochs for systems that contain spectroscopic binaries that may be observed at a more favorable orbital phase.
- Coverage of the separation-magnitude difference ($d - \Delta m$) plane to test the limitations of the technique and comparison with other techniques (STIS I).
- Exploration of systems with spectral types significantly different to the relatively narrow scope of LS I.
- Extension of the technique to systems with fainter primaries.

In this paper we present our results for 19 close visual binaries observed with lucky spectroscopy (one from the previous sample and 18 new ones, Table 1), which were selected

Table 3. Measurements for visual pairs using our AstraLux lucky images. The evening date, Heliocentric Julian Date (HJD), separation (d), position angle (θ), and magnitude difference is given in each case. Six different filters were used: Johnson V , $H\alpha$, SDSS i and z , zn (a narrow filter with a central wavelength similar to that of z), and Y , in order of increasing central wavelength.

Pair	Even. date (YYMMDD)	HJD–2 400 000 (d)	d ($''$)	θ (deg)	ΔV (mag)	$\Delta H\alpha$ (mag)	Δi (mag)	Δz (mag)	Δzn (mag)	ΔY (mag)
FN CMa A,B	121002	56 203.70	0.577±0.005	115.58±0.11	1.66±0.02	...
	181126	58 449.63	0.581±0.005	115.39±0.11	1.63±0.02	...
6 Cas A,B	121002	56 203.52	1.497±0.003	195.69±0.04	2.45±0.01	3.05±0.01
	130918	56 554.63	1.496±0.003	195.81±0.06	2.78±0.02
α Sco A,B	190615	58 650.44	2.743±0.021	276.96±0.23	...	6.09±0.07	7.45±0.11	8.01±0.10
σ Sco Aa,Ab	190616	58 651.40	0.423±0.003	217.17±0.22	2.10±0.09	2.25±0.07
CS Cam A,B	181227	58 480.41	2.316±0.002	162.12±0.05	4.62±0.03	4.66±0.08
HD 5005 A,B	071112	54 417.44	1.526±0.002	82.12±0.04	1.59±0.01
	130918	56 554.64	1.526±0.002	82.25±0.04	1.60±0.01
	181127	58 450.36	1.526±0.002	82.19±0.04	1.57±0.01	1.59±0.01
HD 51 756 A,B	121013	56 204.69	0.705±0.001	102.94±0.04	0.29±0.01
	130919	56 555.69	0.706±0.001	102.83±0.04	0.32±0.01
HD 218 195 A,B	110913	55 818.48	0.944±0.001	80.01±0.07	2.66±0.04
	130918	56 554.52	0.943±0.001	80.01±0.08	2.69±0.03
HD 219 460 A,B	110913	55 818.45	1.371±0.001	128.00±0.04	−0.12±0.01
	130918	56 554.48	1.370±0.001	128.08±0.04	−0.04±0.01
HD 8768 A,B	081021	54 761.63	0.662±0.002	27.97±0.34	2.62±0.09
	110913	55 818.50	0.658±0.002	28.42±0.18	2.73±0.04
	130918	56 554.65	0.657±0.004	28.57±0.15	2.86±0.14
BD +60 544 A,B	180918	58 380.59	1.948±0.001	168.51±0.04	0.76±0.02
HD 17 520 A,B	080118	54 484.38	0.317±0.001	298.72±0.07	0.69±0.01
	130918	56 554.66	0.320±0.001	299.05±0.08	0.71±0.02
HD 24 431 A,B	080118	54 484.41	0.734±0.001	177.18±0.15	2.83±0.09
	110913	55 818.59	0.737±0.004	176.65±0.11	3.10±0.17
HD 164 492 A,B	130919	56 555.30	6.261±0.001	20.37±0.04	3.01±0.05
HD 164 492 A,C	130919	56 555.30	10.707±0.008	211.93±0.04	1.35±0.05
HD 164 492 A,H	130919	56 555.30	1.489±0.019	345.03±0.10	5.21±0.19

with those points in mind. The setup and technique used are the same as in LS I with one difference. In that first paper we used the standard CCD for the blue arm of ISIS, an EEV12 array of 2048×4096 13.5 μm pixels. Here we used that CCD as the default setup but we also tried the alternative QUCAM3 CCD for the faint range of our sample. QUCAM3 is an electron-multiplying CCD with 1024×1024 13 μm pixels with a fast mode that has very little readout noise (that we did not use) and a standard slow mode in which it operates as a normal CCD (the one we used). The big advantage of QUCAM3 with respect to EEV12 is that it is a full-transfer device that allows for a quick transfer (20 milliseconds) of the accumulated charge (the image) into a temporary on-chip storage to be effectively read in 0.66 s (for the detector setup used for these data) while the detector remains actively acquiring data. (see http://www.ing.iac.es/Astronomy/instruments/isis/L3spectroscopy_v4.html). Therefore, for one-second exposures the dead time is just ~2% while for EEV12 the corresponding dead time is ~14 s, introducing a factor of nearly 15 in the efficiency in favor of QUCAM3. A second, less important, advantage of QUCAM3 is a slightly better pixel scale (0 $''$.19 pixels vs. 0 $''$.20 pixels). The main disadvantage of QUCAM3 arises from its smaller number of pixels: with EEV12 we can cover the 3900–5500 \AA range with a single grating position while with QUCAM3 to cover just the 3900–5100 \AA range we need three grating positions. Those characteristics translate into different observing sequences for the two setups. For EEV12 we have to:

- Acquire the target and place the slit in the correct position angle (typically 4 m).
- Obtain 100 exposures of 1.0 s each in a single grating position (25 m).

- Do an arc (1 m).

That yields 30 minutes/object and 100 s of total exposure time, of which we typically end up using 10–50 s. For QUCAM3 we have to:

- Acquire the target and place the slit in the correct position angle (typically 4 m).
- Obtain 500 exposures of 1.0 s each in the first grating position (8.5 m).
- Do an arc and change to the second grating position (1.5 m).
- Obtain 500 exposures of 1.0 s each in the second grating position (8.5 m).
- Do an arc and change to the third grating position (1.5 m).
- Obtain 500 exposures of 1.0 s each in the third grating position (8.5 m).
- Do an arc and change to the first grating position (1.5 m).

That yields 34 minutes/object, a similar amount to the previous one, but with 500 s of total exposure time as opposed to 100 s (QUCAM3 has a slightly lower quantum efficiency than EEV12 but that effect is small). Therefore, one would expect QUCAM3 to be a more appropriate setup for faint stars, where the S/N per frame is low. For bright stars, the advantage is lost because the S/N per frame is high and EEV12 has the advantages of being a simpler setup (less chances of making mistakes or having variable quality issues as a function of wavelength); covering a larger wavelength range; being easier to schedule as it is the default detector for the instrument; and, for the brightest objects such as some of the ones in LS I, the possibility of having exposure times of 0.1 s for the very bright stars (avoiding saturation), which is not allowed in QUCAM3 as the minimum exposure time is set by the readout time of the image. We test the hypothesis about faint stars below with one example.

source with no parallax in *Gaia* DR2. To estimate its distance we assume that it is the same as component C in the system. FN CMa C (*Gaia* DR2 3 046 209 991 397 371 392) has a parallax of 0.6844 ± 0.0509 mas and a RUWE of 0.98. For its distance we use the Bayesian prior described by Maíz Apellániz (2001, 2005) with the updated Galactic (young) disk parameters from Maíz Apellániz et al. (2008), apply a parallax zero point of 0.040 ± 0.010 mas (Maíz Apellániz et al., accepted in A&A), and obtain $1.48^{+0.12}_{-0.11}$ kpc.

We attempted to separate the two components of the system in three occasions and were successful in two of them (Fig. 1). The primary is indeed an early B star but of later spectral subtype (B0.7) and higher luminosity class (Ib) than claimed by Rivinius et al. (2011). The secondary is indeed an O6 dwarf but with z suffix, thus likely underluminous for its spectral classification (Arias et al. 2016). These differences with the Rivinius et al. (2011) classifications explain the Δm between the two components and allow them to be at the same distance, a more likely arrangement than a chance alignment between two such bright stars. Note how the two components are cleanly separated, with no sign of He II $\lambda 4542$ in the primary or of Si III or O II lines in the secondary and with radically different (but expected for their spectral types) behaviors in the 4630–4650 Å region. No appreciable differences are seen between the two epochs (but see below for the high-spectral-resolution results). The combined spectrum (top one in Fig. 1) can be classified as B0.2 III: but some peculiarities are seen in it that point towards a composite nature, such as the inability to consistently fit the Balmer profiles and the Si lines at the same time. This is a good example of the advantage of lucky spectroscopy (spatial disentangling) over spectral disentangling, as the latter can introduce artifacts that lead to erroneous spectral characterizations. In this particular case, we suspect that in the Rivinius et al. (2011) disentangling some He II $\lambda 4542$ may have remained in the spectrum of the primary (but as they did not publish the disentangled spectra we cannot be certain).

We have also observed this system with lucky imaging (Table 3). The separations and position angles are compatible with the WDS data but the magnitude difference is just barely so: *Hipparcos* gives $\Delta H = 1.357$ mag and we only expect a color term of ~ 0.1 mag with z photometry. There is no appreciable motion in the 6-year span between the two epochs and there is no obvious trend when considering the positions in the WDS catalog that stretch to over a century ago.

We have nine epochs of this system in the high-resolution (A+B combined) LiLiMaRlin spectra. The He II lines (which originate mostly in the O star) do not show profile changes or velocity shifts. The Si III lines (which originate mostly in the B supergiant) show velocity shifts and the He I lines (which originate in both but mostly in the B supergiant) show profile variations and/or velocity shifts. This is consistent with the finding by Rivinius et al. (2011) that the B-type star is an SB1 with a 117.55 ± 0.33 d period, making FN CMa a quadruple system (including the C component 18'' away).

3.2. 6 Cas A,B, the only known O star with an A supergiant companion

This fifth magnitude system, also known as HD 223 385 A,B, was classified as A3 Ia + sec by Morgan et al. (1953), where we explicitly add “sec” to indicate that the plus sign does not refer to a hypergiant classification (a common source of confusion, note that hypergiants had not been

Table 4. *Gaia* DR2 astrometric data for four stars in the vicinity of 6 Cas with similar parallaxes and proper motions and their aggregate results. The aggregate results use external uncertainties and include the spatial covariance terms of Lindegren et al. (2018).

<i>Gaia</i> DR2 ID	ϖ (mas)	μ_{α^*} (mas/a)	μ_{δ} (mas/a)
2 012 942 869 740 260 096	0.3233 ± 0.0319	-3.600 ± 0.046	-1.781 ± 0.043
2 012 942 805 332 107 136	0.3457 ± 0.0189	-3.417 ± 0.030	-1.421 ± 0.028
2 012 942 496 094 500 096	0.3272 ± 0.0257	-3.442 ± 0.039	-1.387 ± 0.035
2 012 942 564 813 963 264	0.3628 ± 0.0263	-3.569 ± 0.041	-1.479 ± 0.038
	0.3428 ± 0.0402	-3.482 ± 0.063	-1.465 ± 0.063

introduced at the time). The B companion is currently listed in the WDS catalog with $d = 1''5$, PA = 194°, and $\Delta m = 2.29$ mag measured in 2015. Talavera & Gómez de Castro (1987) were the first to suggest that the A supergiant had an O-type companion based on the composite UV spectrum but favored a spectroscopic, not a visual binary. The two components have separate entries in *Gaia* DR2 but their parallaxes cannot be used to derive precise distances: that of A is negative and that of B has a RUWE of 5.15, indicating poor astrometric quality, likely caused by the proximity of the A component. The *Gaia* DR2 ΔG should be reliable, with a value of 2.529 ± 0.016 mag for the A,B pair, but the ΔG_{BP} and ΔG_{RP} are likely not, as they are measured by aperture photometry and the two components are too close. The *Gaia* DR2 positions yield a separation of $1''5016$ and a position angle of 195.89°.

As we cannot use the *Gaia* DR2 data for 6 Cas A,B to obtain a reliable distance to the system, we looked for nearby stars that may be associated with it. The WDS catalog lists a C component but it has a RUWE of 3.87, so we cannot use it. Instead, we use a variation of the method used in Maíz Apellániz (2019). We start with the *Hipparcos* proper motion for 6 Cas and we search for *Gaia* DR2 stars in the vicinity with (a) similar proper motions, (b) good RUWE, (c) G magnitudes brighter than 15, (d) similar blue colors, and (e) self-compatible parallaxes. We found four of those, listed in Table 4. We combine their parallaxes using the technique described in Campillay et al. (2019), including the use of external uncertainties and a spatial covariance term (Lindegren et al. 2018), and apply the same parallax zero point and prior as before. The resulting distance to that group of stars is $2.78^{+0.37}_{-0.29}$ kpc, which we will use here for 6 Cas itself.

We successfully separated the two components of this system on eight occasions with lucky spectroscopy. As no significant variations in the spectral types were observed between epochs, we only plot in Fig. 2 one lucky spectroscopy epoch (including the combined spectrum) along with another epoch of the system where we were able to obtain separate spectra with FRODOSpec@LT (regular GOSSS spectroscopy). The two spectra are cleanly separated despite their very different spectral types with no sign of cross-contamination. 6 Cas B has an O9.5 II spectral type with no sign of any anomaly. The effect of the B component on the combined spectrum is very weak and only shows up in a few lines such as Si IV $\lambda 4089$, C III $\lambda \lambda 4647, 4650, 4651$, He II $\lambda 4686$, and He I $\lambda 4713$ located in wavelength regions without strong lines from the A supergiant. The FRODOSpec spectrograms indicate that this system can also be resolved with regular spectroscopy but at a cost. While the two spectra for the A component in Fig. 2 are nearly identical in spectral resolution and S/N, the lucky spectrogram for the B component has a higher S/N than its regular counterpart due to the reduced noise introduced in the spatial disentangling process.

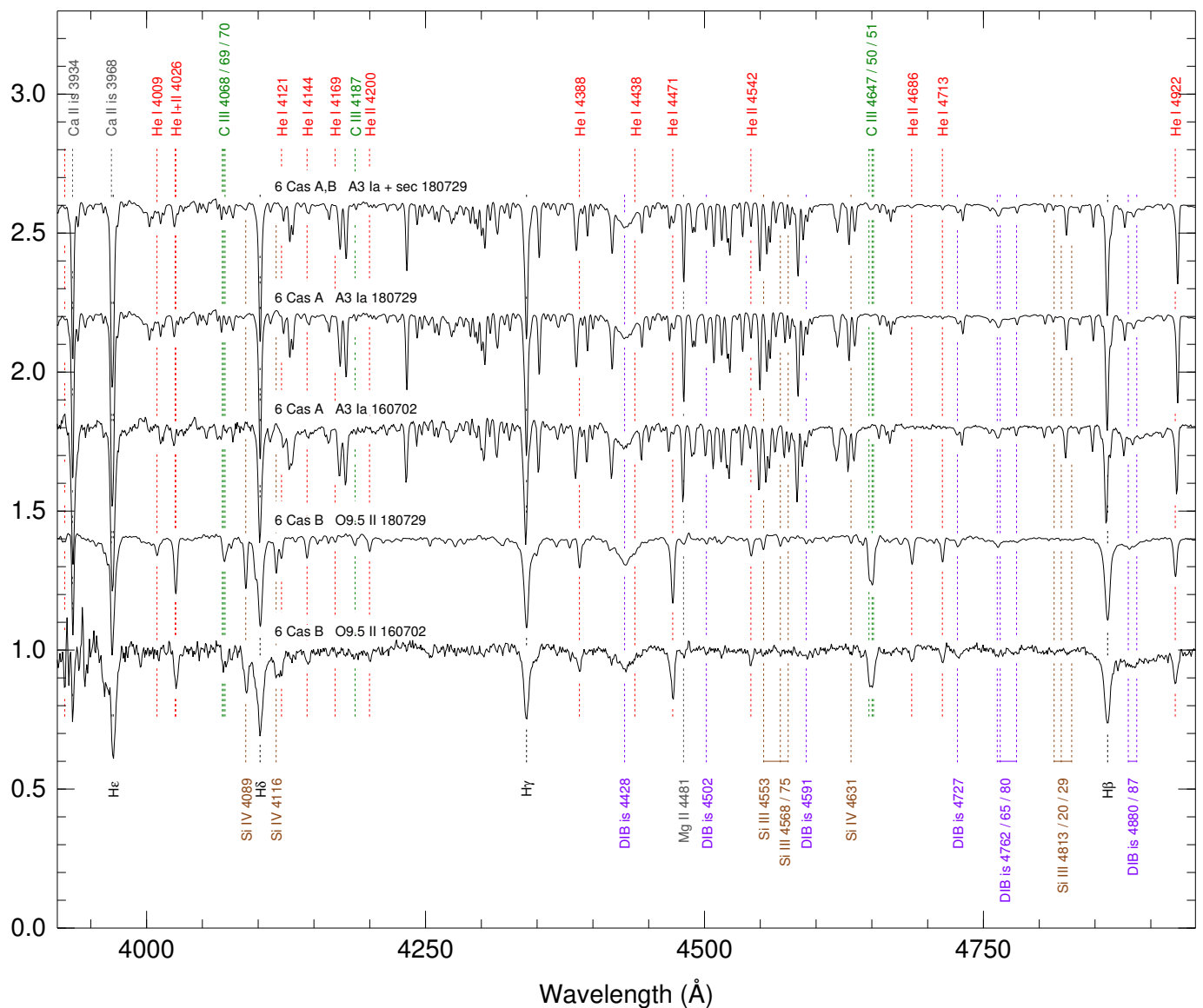


Fig. 2. Rectified spectrograms for 6 Cas at the GOSSS spectral resolution of $R \sim 2500$ and on the stellar reference frame. For each spectrogram, the name, spectral type, and evening date (YYMMDD) are shown. The 160702 data were obtained with FRODOSpect@LT i.e. not with lucky spectroscopy. The top spectrogram is the weighted combination of the two components for the 180729 epoch. Main atomic and ISM lines are indicated.

We have two lucky-imaging epochs of this system (Table 3) spaced by a year and obtained prior to the average *Gaia* DR2 reference epoch (2015.5). Combining those points with the historical data in the WDS catalog, there is little indication of a secular motion, except perhaps in the inward direction, with most observations from the nineteenth century and the beginning of the twentieth having separations of $1''.6$ – $1''.7$. The observed magnitude differences in our lucky images are consistent with the ΔG value above and the spectral types.

We have 12 LiLiMaRlin epochs covering from 2001 to 2020. The lines of the A supergiant show radial velocity variations with a peak-to-peak amplitude of ~ 10 km/s. The motion is not secular but shows variations on time scales of days, pointing towards pulsations as the likely culprit. The phenomenon was already noticed by Aydin (1979). The signature of the B component is difficult to detect in the LiLiMaRlin spectra because of the additional dilution caused by $1''.5$ separation and the circular aper-

tures of less than $3''$ diameter used by échelle spectrographs. In some of our epochs, however, He II $\lambda 5412$ is clearly visible.

3.3. α Sco A,B, the nearest RSG+B system

There are over a hundred known red supergiant stars with B-type companions in the Galaxy (Pantaleoni González et al. 2020), of which α Sco (Antares) is the closest one, with a *Hipparcos* distance (α Sco is not present in *Gaia* DR2) of 187^{+44}_{-30} pc (Maíz Apellániz et al. 2008). The companion was classified as B3 already one century ago (Adams & Joy 1921) and subsequent authors classified it as B4 V (Stone & Struve 1954), B2.5 V (Garrison 1967), and B3 V (Corbally 1984). The differences in classification likely do not reflect real spectral variations but are rather a consequence of the difficulty that exists in eliminating the light from the much brighter primary less than $3''$ away. The B star has not received much attention in the last decades other than the study of its associated emission nebula rich in [Fe II] lines

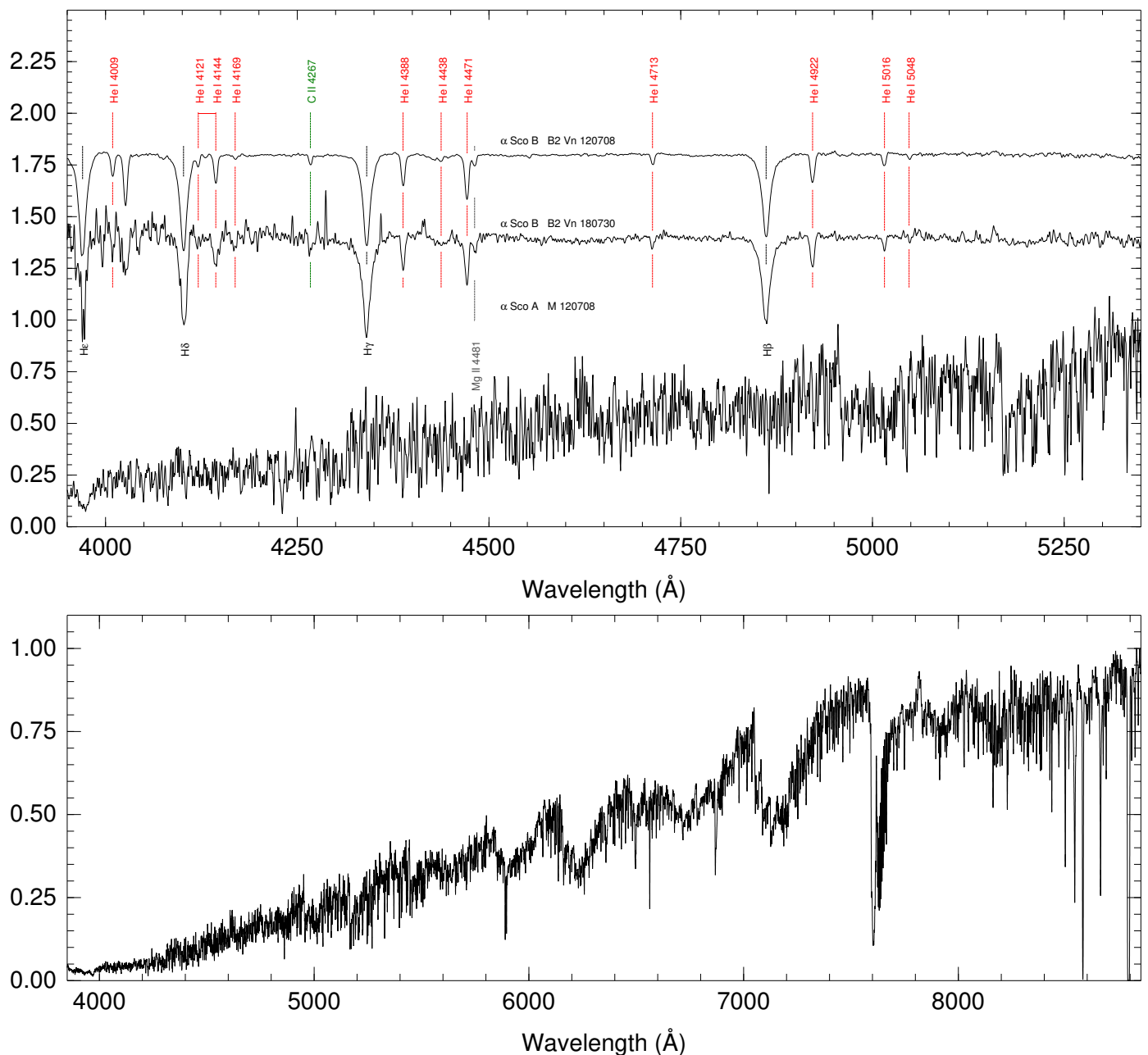


Fig. 3. (Upper panel) Lucky spectrograms for α Sco at the GOSSS spectral resolution of $R \sim 2500$ and on the stellar reference frame. For each spectrogram, the name, spectral type, and evening date (YYMMDD) are shown. The 120730 data were obtained with a position angle offset of 24° from the A,B line and the 180730 data were obtained with the slit aligned with the A,B line. The spectra of the B component have been rectified while the spectrum of the A component has been dereddened and relative-flux calibrated. Main atomic lines are indicated. (Lower panel) α Sco A spectrogram from LiLiMaRlin degraded to $R \sim 4000$, relative-flux calibrated, and not corrected for telluric absorption.

(Swings & Preston 1978; Reimers et al. 2008). The magnitude difference between the two components is highly dependent on the band used (see below), as expected for a pair composed of a red and a blue star (this pair is a favorite object among amateur astronomers who want to separate visual binaries of extreme colors and small separations, the first author still remembers his excitement when he was able to separate Antares through an eyepiece for the first time 34 years ago).

We observed α Sco A,B with lucky spectroscopy on four occasions and we were successful in all of them but with very different values of the S/N for the B component, an effect likely caused by the large magnitude difference. We measure that value in our data to be ~ 3.6 mag in the B band but with a significant

difference between 4000 \AA and 5000 \AA . Of the four epochs, the one with the best seeing (and consequently higher S/N) is the first one from 2012, when we first attempted lucky spectroscopy with ISIS@WHT. On that occasion we centered the slit on the B component and used a position angle offset of 24° with respect to the A-B line. This reduces the effective separation slightly but it is heavily compensated by the effect of making the flux from the two components similar in the B band, which is the most important constraint in this case (see Table 1). We classify the B component as B2 Vn, which differs from previous results in two ways: the spectral subtype is earlier and the star shows a significant line broadening likely caused by rotation. We used the semi-automatized tool iacob-broad to measure the projected

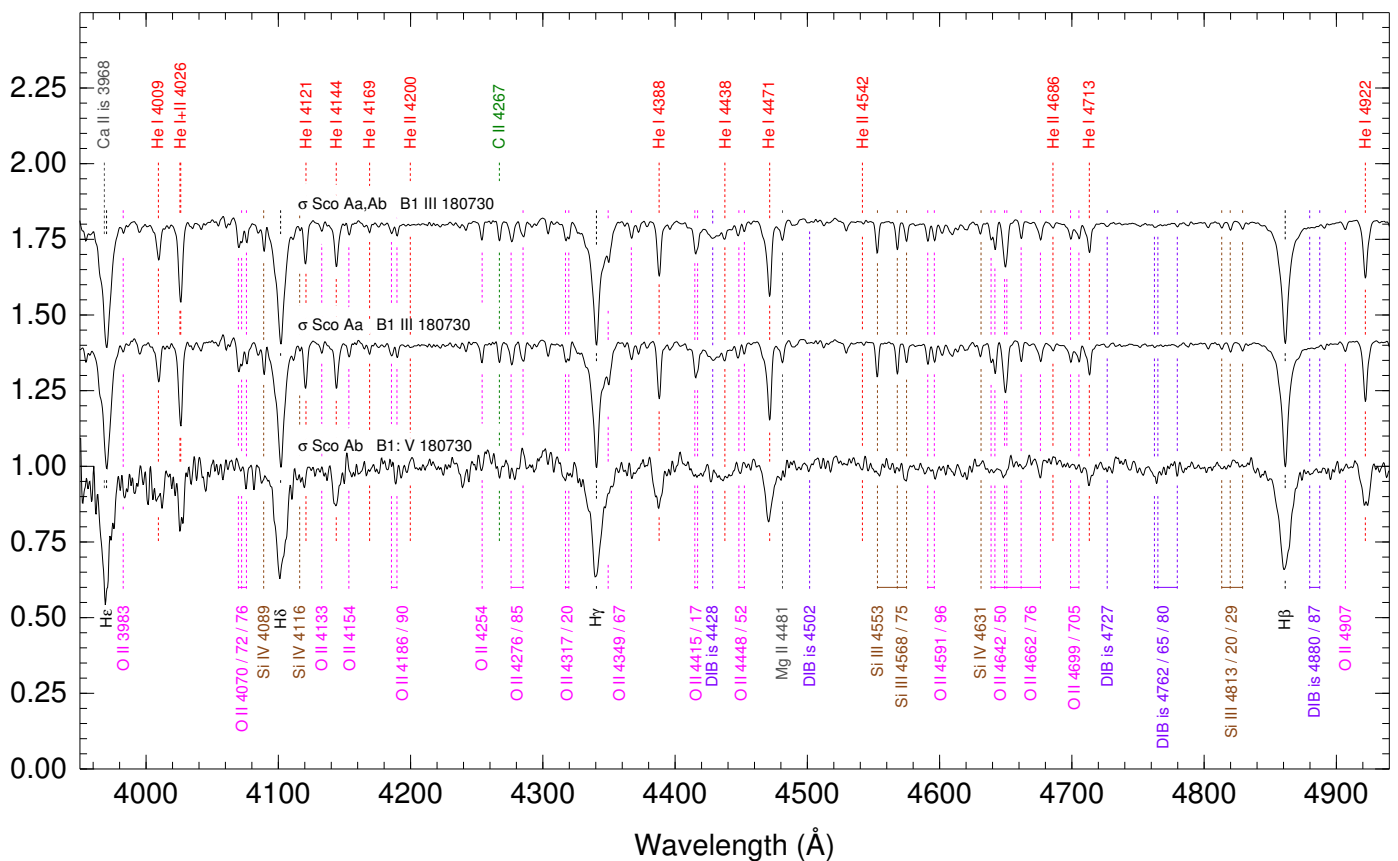


Fig. 4. Rectified spectrograms for σ Sco at the GOSSS spectral resolution of $R \sim 2500$ and on the stellar reference frame. For each spectrogram, the name, spectral type, and evening date (YYMMDD) are shown. The top spectrogram is the weighted combination of the two components for the 180730 epoch. Main atomic and ISM lines are indicated.

rotational velocity ($v \sin i$) from a combined Fourier transform plus goodness-of-fit technique (see Simón-Díaz & Herrero 2014 and references therein) using the top spectrum in Fig 3. The absence of strong metallic lines, due to the significant line broadening, made us rely on He I lines. This means the Stark broadening effect needs to be considered and, therefore, the amount of macroturbulent broadening cannot be adjusted. From the fitting of four different lines (He I λ 4387, He I λ 4471, He I λ 4713, and He I λ 4922) and the agreement between results obtained by both techniques used as consistency check (see e.g. Berlanas et al. 2020) we obtain a $v \sin i$ for the B component of 260 ± 30 km/s. In this way, α Sco B is another example of a massive-star companion with a high rotation (see LS I and STIS I).

Morgan & Keenan (1973) selected α Sco A as the MK M1.5 Iab standard, although Keenan & McNeil (1989) later gave it a slightly lower luminosity at M1.5 Iab-Ib. There are many spectral classifications in the literature indicating earlier types, but the strength of the TiO band system in the spectrum rules them out. We have used the Mercator spectrogram from LiLiMaRlin shown in Fig. 3 to classify α Sco A following the procedures described in Dorda et al. (2018) and their set of standards at $R = 4000$. Direct comparison to HD 206 936 (M2 Ia) and HD 36 389 (M2 Iab-Ib) shows all the temperature sensitive TiO bandheads to be essentially identical in α Sco A, although α Ori, nominally M1-2 Ia-Iab, has very slightly stronger bands. The strength of the Ca II triplet and other luminosity indicators in its range agree well with those in the blue, and we consider the M1.5 Iab classification fully justified but noting the difficulty in distinguishing between M1.5 and M2.

We have one lucky imaging epoch of α Sco. The WDS catalog contains data on the system that spans a century and three quarters but the dispersion is large, likely an effect of the large magnitude difference between A and B. There is some evidence of a small inward and counterclockwise motion over that time span but the period must be of at least several thousands of years.

3.4. σ Sco Aa,Ab, a spectral classification and extinction standard

This is a well-known object that was used as one of the spectral classification standards for B1 III by Johnson & Morgan (1953). More recently, it has also been used as an extinction standard as it is the prototype of σ -type sightlines (Krelowski et al. 1997; Cami et al. 1997; Maíz Apellániz 2015) in a similar way as ζ Oph is the prototype of ζ -type sightlines. σ -type sightlines correspond to relatively lower-density regions of the ISM exposed to UV radiation while ζ -type sightlines correspond to higher-density regions of the ISM shielded from UV radiation. This division was initially applied to diffuse interstellar bands but it has been recently discovered that a broad interstellar feature preferentially appears on σ -type sightlines (Maíz Apellániz et al. 2020, accepted in MNRAS). There is no entry for this target in *Gaia* DR2 but from the *Hipparcos* data and the Maíz Apellániz et al. (2008) prior we derive a distance of 222^{+34}_{-26} pc. Alternatively, North et al. (2007) derive a distance of 174^{+23}_{-18} pc from the Aa1,Aa2 orbit (see below).

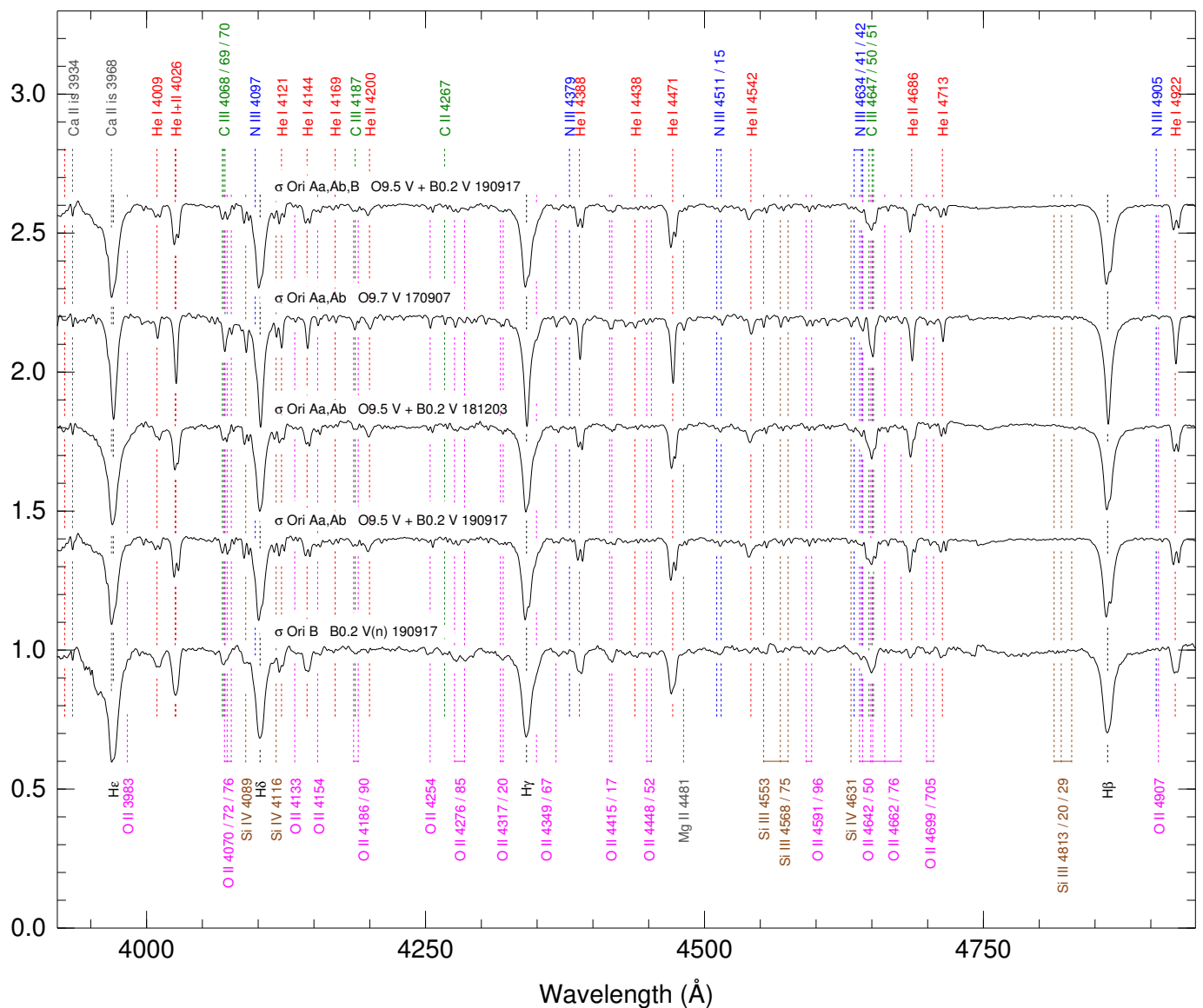


Fig. 6. Rectified spectrograms for σ Ori at the GOSSS spectral resolution of $R \sim 2500$ and on the heliocentric reference frame. For each spectrogram, the name, spectral type, and evening date (YYMMDD) are shown. The top spectrogram is the weighted combination of the two components for the 190917 epoch. Main atomic and ISM lines are indicated.

located $2''.3$ away and with a 3.6 mag difference in the Tycho-2 bands. The companion has been mostly ignored in the literature. The *Gaia* DR2 parallax for A combined with the Maíz Apellániz et al. (2008) prior and the previously used zero point leads to a distance of 813^{+208}_{-138} pc. The B component also has an entry in *Gaia* DR2 but its RUWE is larger than 1.4.

We successfully spatially separated CS Cam A,B twice with lucky spectroscopy. We show the results for one of the epochs in Fig. 5). The A component appears as a B9 Ia, as expected from the literature. We classify the B component as a B2 III, earlier and less luminous, which is its first ever spectral classification. In the combined spectrum there is no sign of the secondary, other than very slight changes in some He I lines that would go easily unnoticed, at least at this spectral resolution.

There are 35 LiLiMaRlin epochs of CS Cam, where only the A component leaves a significant signal, as B is not only considerably fainter but also outside the aperture in most cases. In the nine years covered by the observations there is no significant motion but a velocity dispersion of 2-3 km/s, a common effect in

B supergiants caused by pulsations (Simón-Díaz et al., submitted to A&A).

We have one lucky imaging epoch of CS Cam. The magnitude differences in the z and Y bands are larger than in the *Hipparcos* H band, which in turn are larger than in the Tycho-2 B and V bands, following the color differences between early- and late-type B stars. The *Gaia* DR2 G magnitude difference is larger but suspect, given the corrections associated with stars that are as bright as CS Cam A (future data releases may change this). The WDS catalog lists pair measurements that go back almost two centuries with no appreciable motion detected but with a considerable scatter in the oldest measurements. Both components appear in *Gaia* DR2 catalog and the astrometric data there are in excellent agreement with our measurements. On the other hand, *Gaia* DR2 detects a relative proper motion mostly in the inward direction that should have accumulated $\sim 0''.4$ over the two centuries of WDS observations. One way to reconcile both results would be if the system has a near edge-on orbit that passed near quadrature a century or so ago.

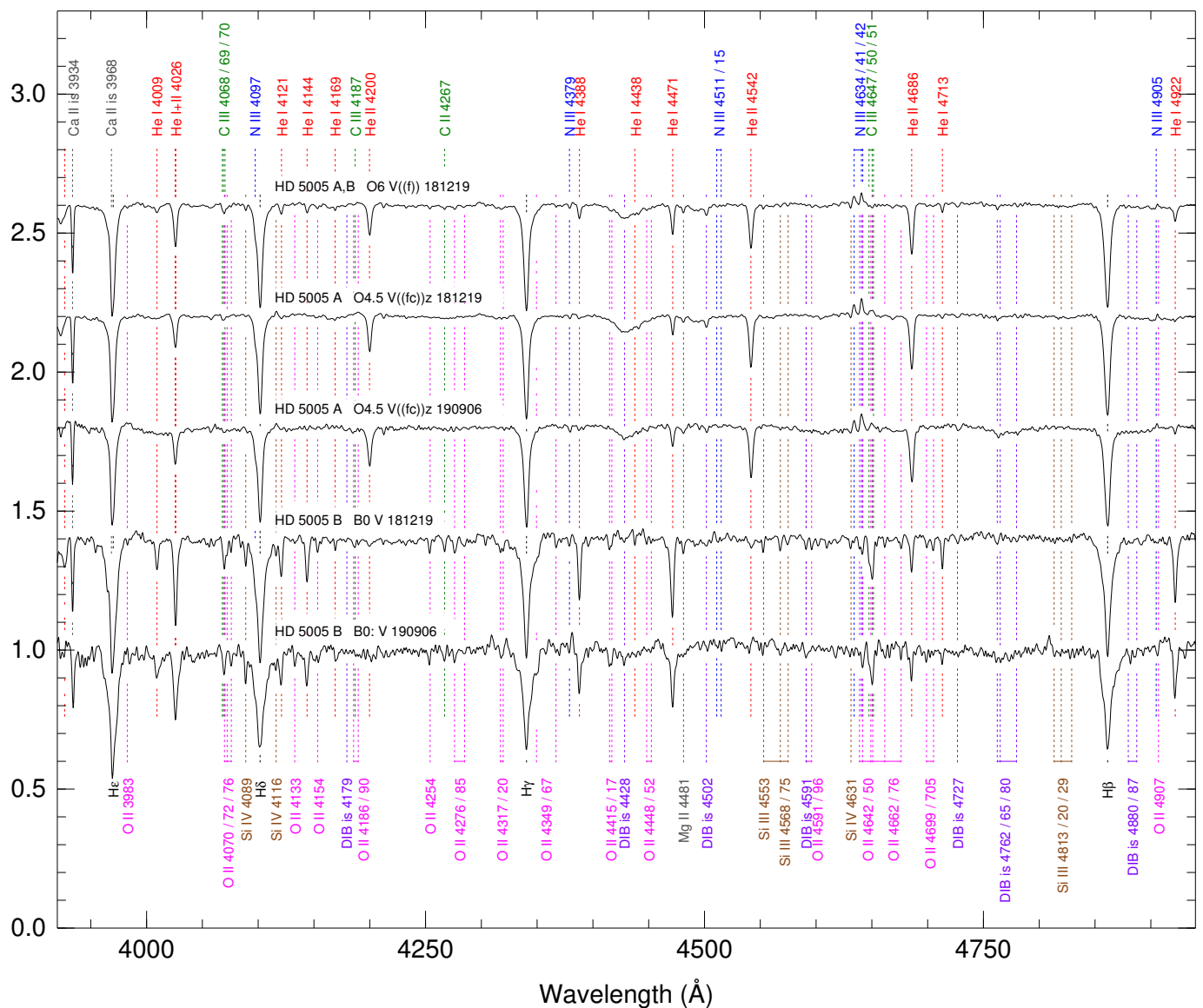


Fig. 7. Rectified spectrograms for HD 5005 at the GOSSS spectral resolution of $R \sim 2500$ and on the stellar reference frame. For each spectrogram, the name, spectral type, and evening date (YYMMDD) are shown. The top spectrogram is the weighted combination of the two components for the 181219 epoch. Main atomic and ISM lines are indicated.

3.6. σ Ori Aa,Ab,B, an epoch with a better velocity separation

This system has been already extensively described in Simón-Díaz et al. (2015a), LS I, and MONOS I, to which the reader is referred for information about it. We presented the first spatially resolved spectra of σ Ori Aa,Ab and σ Ori B in LS I. That observation took place on the night of 170907 (HJD = 2 458 004.74), for which the spectroscopic orbit of Aa,Ab by Simón-Díaz et al. (2015a) predicts a velocity separation of just 15 km/s and, understandably, we were unable to kinematically separate the two components in the spectroscopic binary. In MONOS I we spatially separated the Aa,Ab and B components with a new lucky spectroscopy observation obtained on the night of 181203 (HJD = 2 458 456.54). The prediction for the velocity separation at that time was much more favorable, 234 km/s, and indeed we were able to kinematically separate Aa and Ab and give spectral classifications for each. Here we present new spatially resolved spectra for the night of 190917 (HJD = 2 458 744.69), where the predicted velocity separation

was even larger, 288 km/s, just 1 km/s shy of the maximum value (Fig. 6).

The new spectral classifications are the same as the ones in MONOS I, providing reassurance that once the velocity separation is large enough and lucky spectroscopy is performed under good seeing conditions the result is repeatable. The spectral classification for the combined spectrum Aa,Ab,B is the same as for Aa,Ab, as the large $v \sin i$ of B and the relative similarity between the three spectral types simply creates a dilution of the lines, a point that was already made in Fig. 5 of Simón-Díaz et al. (2015a). The good velocity separation between Aa and Ab allows us to make a precise measurement of the flux ratio between the two of 0.70 ± 0.05 or about 0.4 mag, which is larger than the value in Simón-Díaz et al. (2015a) but not by much. We also note that the latest spectrogram of σ Ori B could be alternatively interpreted as a partially resolved SB2 of two similar stars, given the asymmetry of some lines such as He I $\lambda 4471$, which would make the σ Ori system an SB2+SB2. However, the effect may not be real but the effect of pulsations or of noise in the

spatial disentangling. Further observations may solve the issue, possibly lucky spectroscopy at other phases to detect a larger velocity amplitude in the alleged SB2 or interferometry to spatially resolve it.

3.7. HD 5005 A,B,C,D, a trapezium system with an early-type O star

HD 5005 is a Trapezium system at the core of the IC 1590 cluster that ionizes the NGC 281 H II region, also known as the Pacman nebula. In GOSSS I we classified its four main components (A, B, C, and D) as O stars. In the case of A and B we based the spectral classifications on a spatial disentangling of the two components, which have $d = 1''.6$ and $\Delta m = 1.6$ mag. All four main components have *Gaia* DR2 entries with good values of RUWE so we can combine them in the same way we did for 6 Cas to obtain a distance to HD 5005 of $2.53^{+0.33}_{-0.27}$ kpc.

We have used lucky spectroscopy to spatially separate HD 5005 A,B in two epochs (Fig. 7). The two epochs yield the same spectral classification for the A component, O4.5 V((f)c)z, similar to that of GOSSS I but later by half a spectral subtype and with the z suffix that indicates that He II $\lambda 4686$ is deeper than normal stars with V luminosity class. For the B component we get B0 V for both epochs but with an uncertain spectral subtype for the 190906 epoch due to the lower S/N generated by the spatial disentangling. That spectral classification is later than the O9.5 V from GOSSS I and moves HD 5005 B from the O-star to the B-star category. This is a good example of how lucky spectroscopy allows for a cleaner separation of the spectra of close binaries compared to the traditional, long-exposure methods.

The first lucky spectroscopy epoch (181219) was obtained with the QUCAM3 setup and the second one (190906) with the EEV12 setup. The HD 5005 B QUCAM3 setup has a better S/N, as we suspected from the comparison between the two setups, confirming that it is preferred to the EEV12 one for faint stars. Nevertheless, both setups produce valid and consistent results.

The A,B spectrum in Fig. 7 is of pedagogical value. When one combines the two components (an O4.5 and a B0) we obtain an O6 V((f)) star with no major abnormalities. For example, the C III $\lambda\lambda 4647, 4650, 4651$ triplet is in weak emission in A (hence, the c suffix) and in strong absorption in B. When both are combined (weighted by the Δm), the feature disappears, as expected for a normal O6 dwarf. On the other hand, the N III $\lambda\lambda 4634, 4641, 4642$ triplet, also in emission in A and in absorption in B is left in emission in the combined spectrum (as expected for an object with an ((f)) suffix) because they have similar strengths in each component and the magnitude difference allows the emission to dominate. Therefore, it is possible for such an unresolved binary system to remain undetected in single-epoch spectroscopy with $R \sim 2500$ and to make us believe that the object is a single star of intermediate spectral type.

There are 9 LiLiMaRlin epochs of HD 5005 A,B but the data are complicated to interpret, as the separation between the two components combined with the different apertures for each spectrograph and seeing variations make the contribution of each of the two components different in each epoch. The He II lines, dominated by A, are relatively stable in intensity (and also in velocity, pointing towards the absence of a spectroscopic companion). On the other hand, He I $\lambda 4922$, dominated by the B component (Fig. 7), has large artificial variations in intensity due to that effect. This is a good example of where one needs spatially resolved spectroscopy to study spectroscopic binarity. This system is also of particular interest since is one of the cases in which quantitative spectroscopy leads to the early-O star lying closer

to the ZAMS than the bulk of Galactic O-type stars analyzed by Holgado et al. (2020). Knowing to what extent the B companion is affecting the derived parameters is of prime importance to ascertain the reliability of the differentiated position of this star in the spectroscopic HR diagram.

For HD 5005 we have three good-quality AstraLux epochs, one of them already reported in Maíz Apellániz (2010), that span a period of eleven years. There is no appreciable motion between the A and B components in that time span. This is consistent with the WDS data that go back a century and a half with nearly constant position angles and separations and with the relative proper motion in *Gaia* DR2, which is essentially zero in right ascension and within two sigmas of that value in declination.

3.8. HD 51 756 A,B, a system of two similar components with a new O star

HD 51 756 is a bright but relatively poorly studied early-type system that has spectral classifications listed in Simbad that range in spectral subtype from B0 to B3 and in luminosity class from IV to Ib. It is composed of a pair A,B separated by $0''.7$ and with a small magnitude difference of just 0.3 mag. A third C component is dimmer and located $13''$ away. The A,B pair has no entries in *Gaia* DR2 but the C component has a parallax of 0.5398 ± 0.0575 mas and a good RUWE there. Using the *Gaia* DR2 for the C component as we have done previously for FN CMA we obtain a distance of $1.79^{+0.21}_{-0.17}$ kpc.

We spatially resolve the A and B components with lucky spectroscopy (Fig. 8) and we derive classifications of B0 IV for the first (brighter) component and O9.7 IV(n) for the second (dimmer) component. The two spectral classifications are similar but B is a faster rotator and of an earlier subtype. This is the first time that HD 51 756 B has been identified as an O star and, given its magnitude ($V \sim 8.1$ mag), it is one of the brightest objects of that type identified recently. Note that Roman-Lopes et al. (2018) already indicated that the composite A,B spectrum is O9.7 III and that for the composite we obtain B0 IV instead (Fig. 8), the small difference being likely caused by not matching spectral resolutions between standards and observations, which is a large effect around O9.7/B0 spectral subtypes due to the differences in intrinsic line width between He II $\lambda 4542$ and Si III $\lambda 4552$. This system is similar to FN CMA in that the B star in an O+B pair is capable of hiding the nature of the hotter companion in the unresolved spectrum.

There are 18 LiLiMaRlin epochs for HD 51 756 A,B, where both visual components are included. The line profiles at high resolution show a clearly composite profile, with a narrow component and a broad one, which we assign to A and B, respectively, based on our lucky spectroscopy. The narrow component shows velocity variations with a peak-to-peak amplitude of ~ 20 km/s, suggesting that A is an SB1. If that were the case, it would explain why A is slightly brighter than B despite being one quarter of a spectral subtype later and with the same luminosity class, as the second star (which would be Ab if it were resolved) would contribute to the light without leaving a significant signature in the spectrum (possibly because it is a fast rotator, as B is, note that would make this system quite similar to σ Ori).

We have two lucky imaging epochs for this system and our results agree with those of *Hipparcos* from 1991.25 in terms of separation, position angle, and magnitude difference (there are no entries for this system in *Gaia* DR2). The only slight difference is in position angle, for which there is a small counterclockwise movement that is also consistent with the historical WDS

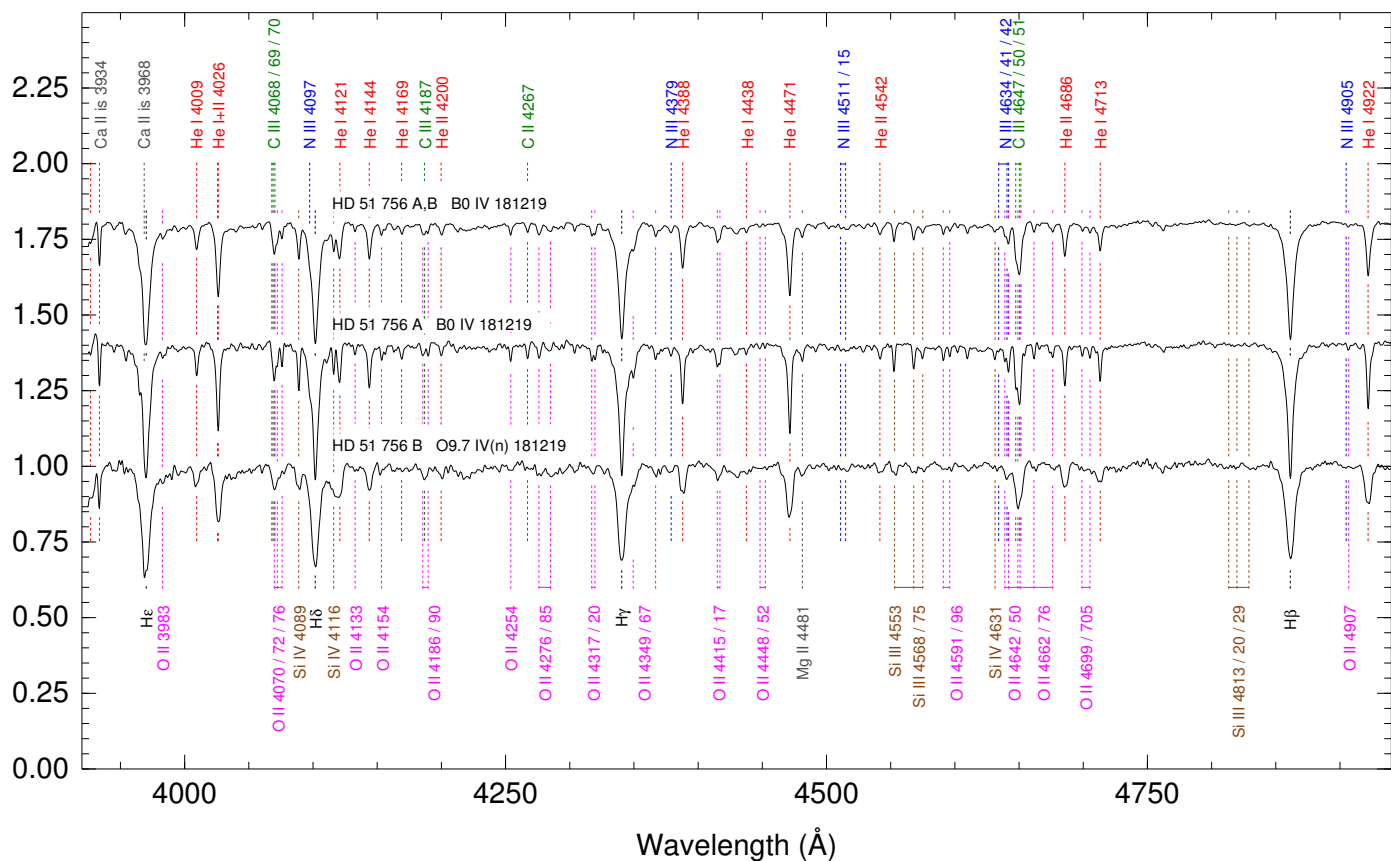


Fig. 8. Rectified spectrograms for HD 51 756 at the GOSSS spectral resolution of $R \sim 2500$ and on the stellar reference frame. For each spectrogram, the name, spectral type, and evening date (YYMMDD) are shown. The top spectrogram is the weighted combination of the two components for the 181219 epoch. Main atomic and ISM lines are indicated.

data that stretches back a century and a half. For a circular face-on orbit the corresponding period is around 7 ka.

3.9. HD 218 195 A,B, a system with a N-rich primary

HD 218 195 A is a nitrogen-enhanced O star (GOSSS II) with a B component located at a separation of $0''.94$ that is 2.7 mag dimmer. The WDS catalog lists two weaker components, C and D, farther away. The A component has an entry in *Gaia* DR2 but with a RUWE of 1.67, so we cannot use its parallax to derive the distance. There is no clearly defined cluster around the object and the C component (*Gaia* DR2 2 010 239 999 586 616 448) also has a high RUWE. Our last resort to obtain a *Gaia* DR2 distance to the system is to assume that the D component (*Gaia* DR2 2 010 239 999 586 619 392, with a RUWE of 0.94), located $11''.4$ away, is physically bound to A,B. If that is the case the distance to the system is $2.29^{+0.20}_{-0.17}$ kpc.

Despite the large magnitude difference, we were able to spatially separate A and B with lucky spectroscopy and obtain a clean spectrum of the weak component. HD 218 195 A maintains the O8.5 IINstr classification of GOSSS II (Fig. 9), as the B component exerts little influence on the combined spectrum at $R \sim 2500$ (but see below for the high-resolution case). The B component, which was already identified as an early-B star in GOSSS I, has a spectral type of B1.5 V. As an indication of the clean separation of the two components, the B spectrum has no

anomalies around the wavelengths where He II lines are seen in the A spectrum.

There are eight LiLiMaRlin epochs for HD 218 195 A,B that span 14 years, with both components included in the aperture. All the strong lines look single and there are no appreciable velocity variations, indicating that the primary has no spectroscopic companions. However, the situation changes when one looks at weak lines where the contribution of the B component dominates despite the large magnitude difference, such as C II $\lambda 4267$ and some O II lines. For those lines there are significant time-dependent changes and at least one epoch shows double profiles with a velocity separation of ~ 70 km/s. We also note that some lines in the B spectrum in Fig. 9 are slightly asymmetric. Therefore, we tentatively identify the B component as an SB2.

We have two lucky imaging epochs for this system, one of them already reported in Maíz Apellániz (2010), and our results are in reasonable agreement with those of *Hipparcos* from 1991.25 in terms of separation, position angle, and magnitude difference. There are few historical observations of this pair in the WDS catalog but the scarce data from the early twentieth century point towards a small secular increase in separation.

3.10. HD 219 460 A, WR 157, disentangling two very different spectra

HD 219 460 is a visual binary whose A component is of B spectral type and its B component is a Wolf-Rayet star

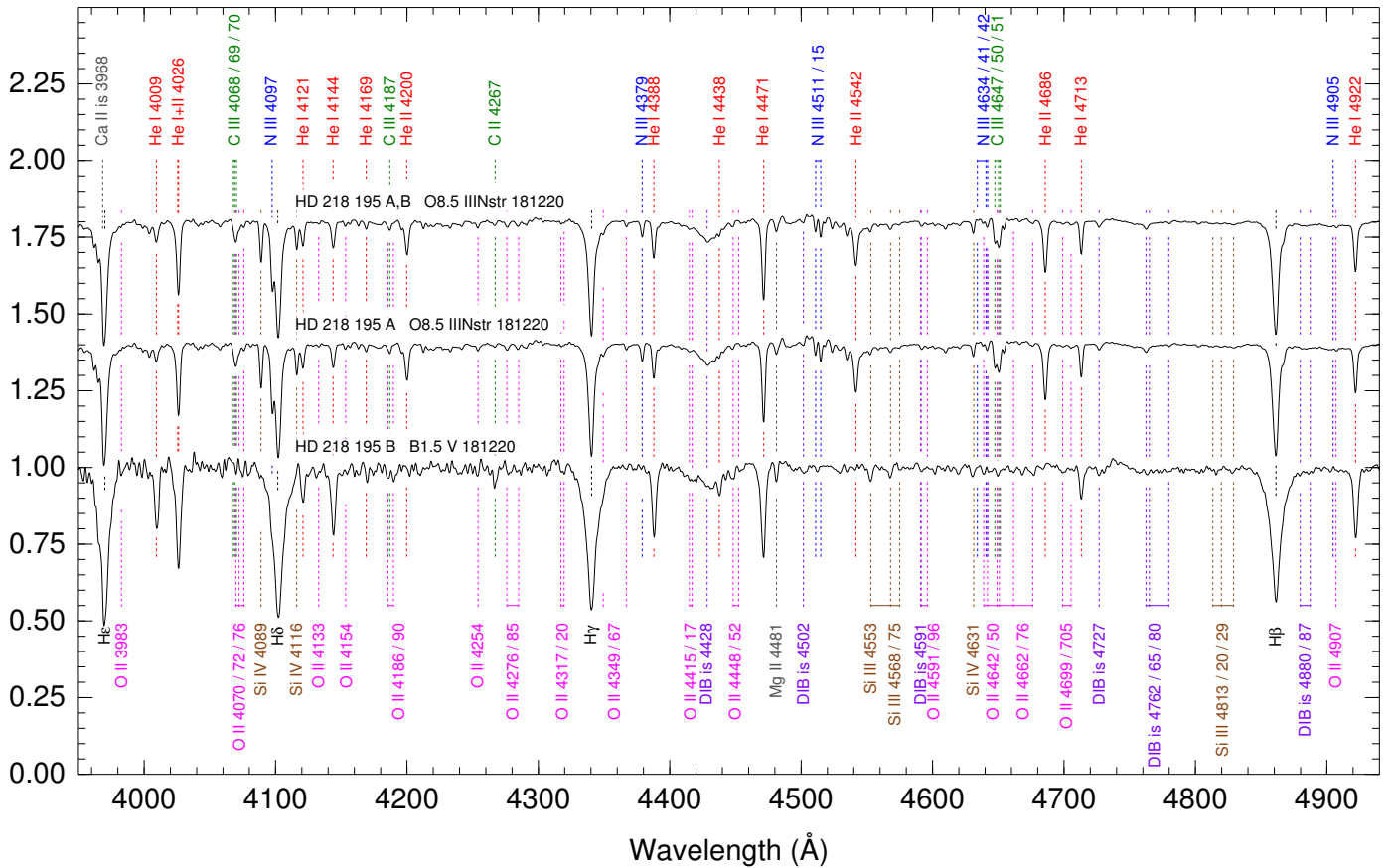


Fig. 9. Rectified spectrograms for HD 218 195 at the GOSSS spectral resolution of $R \sim 2500$ and on the stellar reference frame. For each spectrogram, the name, spectral type, and evening date (YYMMDD) are shown. The top spectrogram is the weighted combination of the two components for the 181220 epoch. Main atomic and ISM lines are indicated.

(WR 157). The system was classified as B1 II + WN4.5 by Turner et al. (1983) based on an spatially unresolved spectrum, something that is feasible because of the very different ionic species and absorption/emission nature of the lines present in an early-B supergiant and a Wolf-Rayet star (Fig. 10). The separation between the two components is $1''.37$ and the magnitude difference is small, with A being 0.4 mag brighter than B in Tycho-2 *B*. Both HD 219 460 A and WR 157 have *Gaia* DR2 entries but the RUWE for the latter is 1.9, prompting us to use the former to calculate the distance. Using the same parallax zero point and prior as before we obtain $2.58^{+0.25}_{-0.21}$ kpc.

Given the small magnitude difference and the relatively large separation, this system is relatively easy to spatially separate with lucky spectroscopy. We point out, however, how clean the disentangling is in Fig. 10: there are no signs of emission lines in the B star and the only absorption lines in the WR star are all caused by the ISM with the only exception of the absorption components in the P-Cygni profiles for N v $\lambda\lambda 4604, 4620$. The absorption lines for the A component are asymmetric and from the narrowest ones (e.g. He I $\lambda 5016$) we identify the system as an SB2 caught with a velocity of ~ 175 km/s. The primary spectroscopic component can be accurately classified as B0.7 II (quite similar to the Turner et al. 1983 result) but the spectral type of the secondary spectroscopic component is more uncertain. Further epochs are necessary to see if the system can be caught with a larger velocity difference. The B component (WR 157) is classified as WN5 according to the criteria for nitrogen lines in Smith et al. (1996), as our spectrum does not reach to He II $\lambda 5412$ or

He I $\lambda 5876$. The composite spectrum in Fig. 10 shows the (diluted) combination of both visual components.

For this system we have two lucky imaging epochs. Our position angles and separations are very similar and are in excellent agreement with the *Gaia* DR2 ones, as both components are also detected there. Our magnitude differences are negative, meaning that WR 157 is brighter than HD 219 460 A in our bands. Indeed, the magnitude difference decreases from Tycho-2 *B* to Tycho-2 *V* to *Gaia* DR2 (all positive) to *i* to *z* (both negative), indicating that the B component is redder than the A component. The *Gaia* DR2 relative proper motion should lead to a counter-clockwise motion of WR 157 with respect to HD 219 460 A of $\sim 6^\circ$ between the early twentieth century and nowadays but no such effect is seen in the average of the two epochs around that time in the WDS catalog.

3.11. HD 8768 A,B, an OC+B visual binary

HD 8768 was classified as O9.5 IV by Morgan et al. (1955), who were unaware of the existence of a B component with $d = 0''.66$ and $\Delta m = 2.6$ mag (Maíz Apellániz 2010). A third C component is located $5''.9$ away but is too faint to make a significant contribution to the spectrum. This object has received little attention in the literature compared to other O stars of similar magnitude. The pair is unresolved in *Gaia* DR2 and with a negative parallax and a RUWE value of 3.2, likely as a result of the different contributions from each component to each observation. The C component, on the other hand, has a valid RUWE

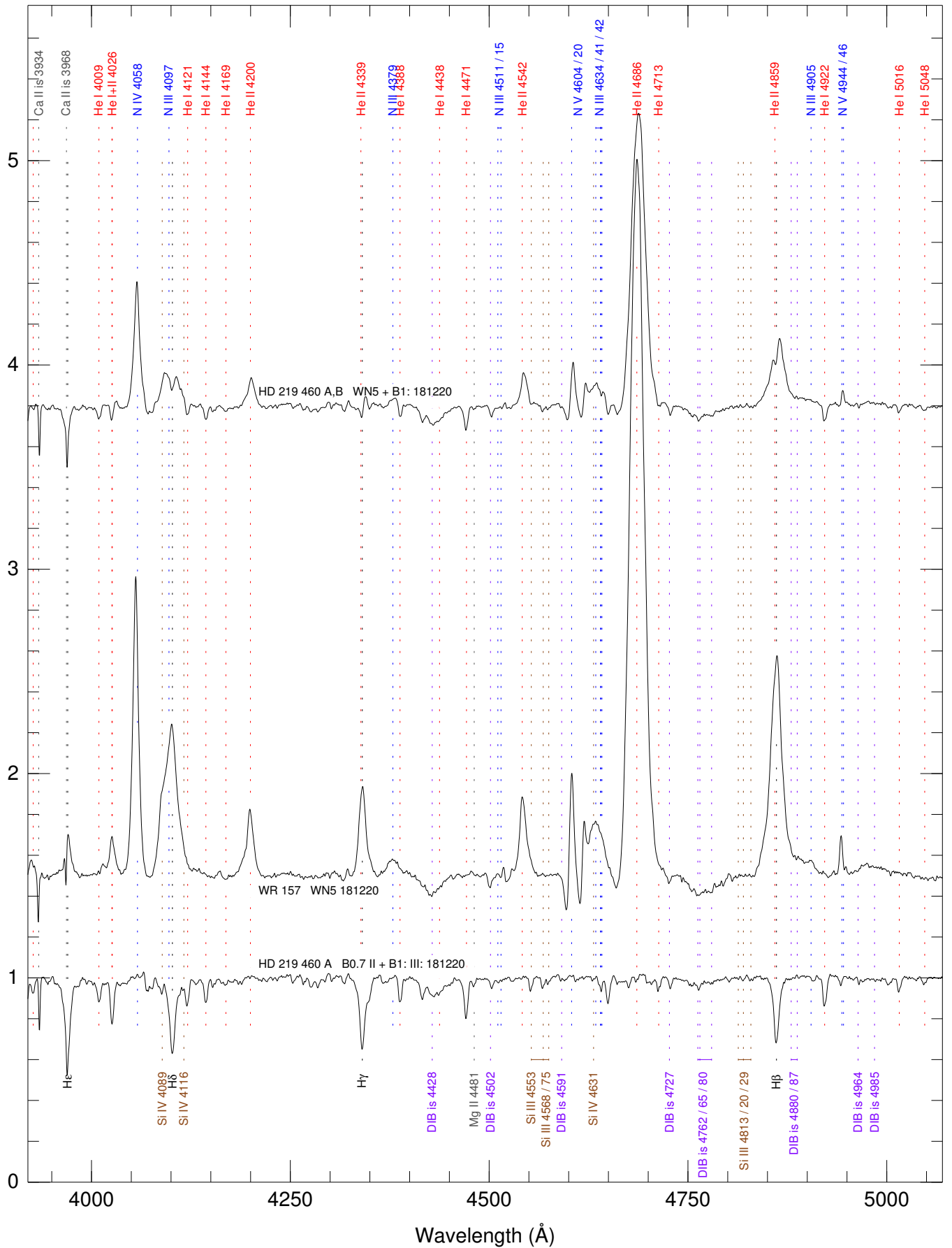


Fig. 10. Rectified spectrograms for HD 219 460 at the GOSSS spectral resolution of $R \sim 2500$ and on the stellar reference frame. For each spectrogram, the name, spectral type, and evening date (YYMMDD) are shown. The top spectrogram is the weighted combination of the two components for the 181220 epoch. Main atomic and ISM lines are indicated.

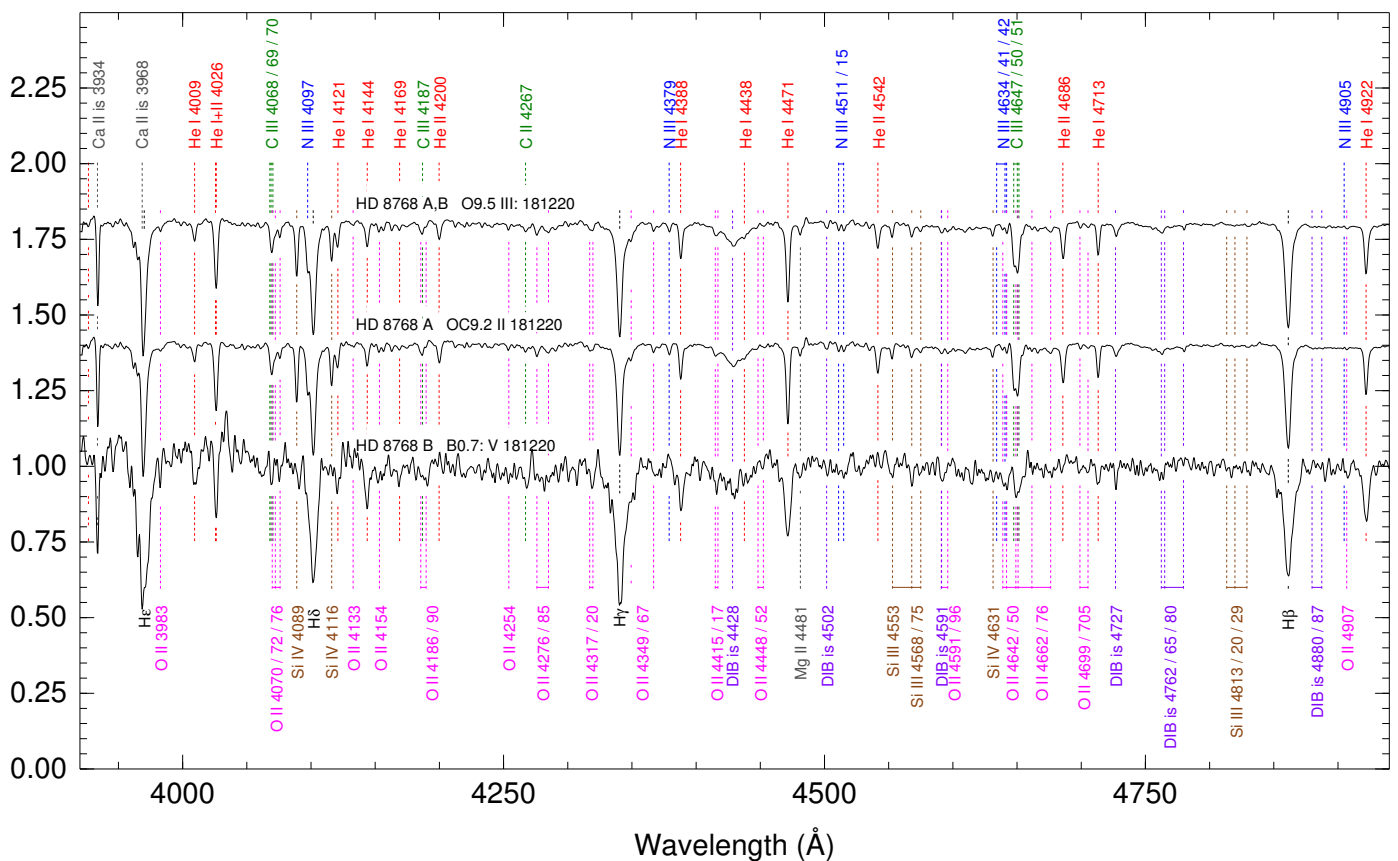


Fig. 11. Rectified spectrograms for HD 8768 at the GOSSS spectral resolution of $R \sim 2500$ and on the stellar reference frame. For each spectrogram, the name, spectral type, and evening date (YYMMDD) are shown. The top spectrogram is the weighted combination of the two components for the 181220 epoch. Main atomic and ISM lines are indicated.

and we can use it to estimate the distance (assuming it is physically associated to the A,B pair) with the same parallax zero point and prior as before to obtain $3.11^{+0.77}_{-0.52}$ kpc.

We spatially separated the A and B components with lucky spectroscopy (Fig. 11). For A we obtain a spectral classification of OC9.2 II, as established by its weak nitrogen lines (e.g. N III $\lambda\lambda 4511, 4515$) and strong carbon lines (e.g. C III $\lambda\lambda 4068, 4069, 4070$), adding in this way a new member to the rare class of carbon-enriched O stars. The spectrogram for B is noisy as a consequence of the small separation and large magnitude difference, but we are able to establish that it is an early-B dwarf with a most likely subtype of B0.7. The combined spectrum shows a small influence of the B component in moving the spectral subtype to O9.5 and leaving an uncertain luminosity classification due to the inconsistency between different classification criteria (a problem common to such combinations of late-O + early-B binaries, see Simón-Díaz et al. 2015a). That effect explains the original classification by Morgan et al. (1955).

We have three lucky imaging epochs of this system, one of them already reported in Maíz Apellániz (2010). That data point and the *Hipparcos* one are the only ones in the WDS catalog, so there is little historical information. Our data show a hint of a counterclockwise motion of B around A but the uncertainties are large, so new epochs are needed to confirm it. The motion corresponds to a period of at least several thousand years.

3.12. BD +60 544 A,B, a new O-type system

This system has no previous accurate spectral classifications listed in Simbad, just two references that indicate it is of OB type (Hardorp et al. 1959; Rydstrom 1978). The WDS catalog indicates it is a pair separated by $1''.9$ with a Δm of 0.9 mag and a first measurement from a century ago. Both components have entries with good RUWE in *Gaia* DR2 and with parallaxes within one sigma of each other. We combine the two with the same zero point and prior as before (and including the covariance term) to obtain a distance of $2.24^{+0.33}_{-0.25}$ kpc.

This system is relatively easy to spatially separate with lucky spectroscopy given its relatively small magnitude difference and large separation (Fig. 12). The A component is classified as O9.5 IV, making this the first time it is identified as an O star. The B component, on the other hand, is classified as B1 V. The merged spectrum receives the intermediate classification of O9.7 IV, with the uncertainty in the luminosity class being another instance of conflicting luminosity criteria when combining a late-O star and an early-B star.

We have one lucky imaging epoch of BD +60 544. Both components are also detected in *Gaia* DR2 and there is good agreement with our values for the separation, position angle, and magnitude difference.

3.13. HD 17520 A,B, a system with an Oe star

This system was analyzed in previous GOSSS papers and in GOSSS III the A component was assigned a spectral type of

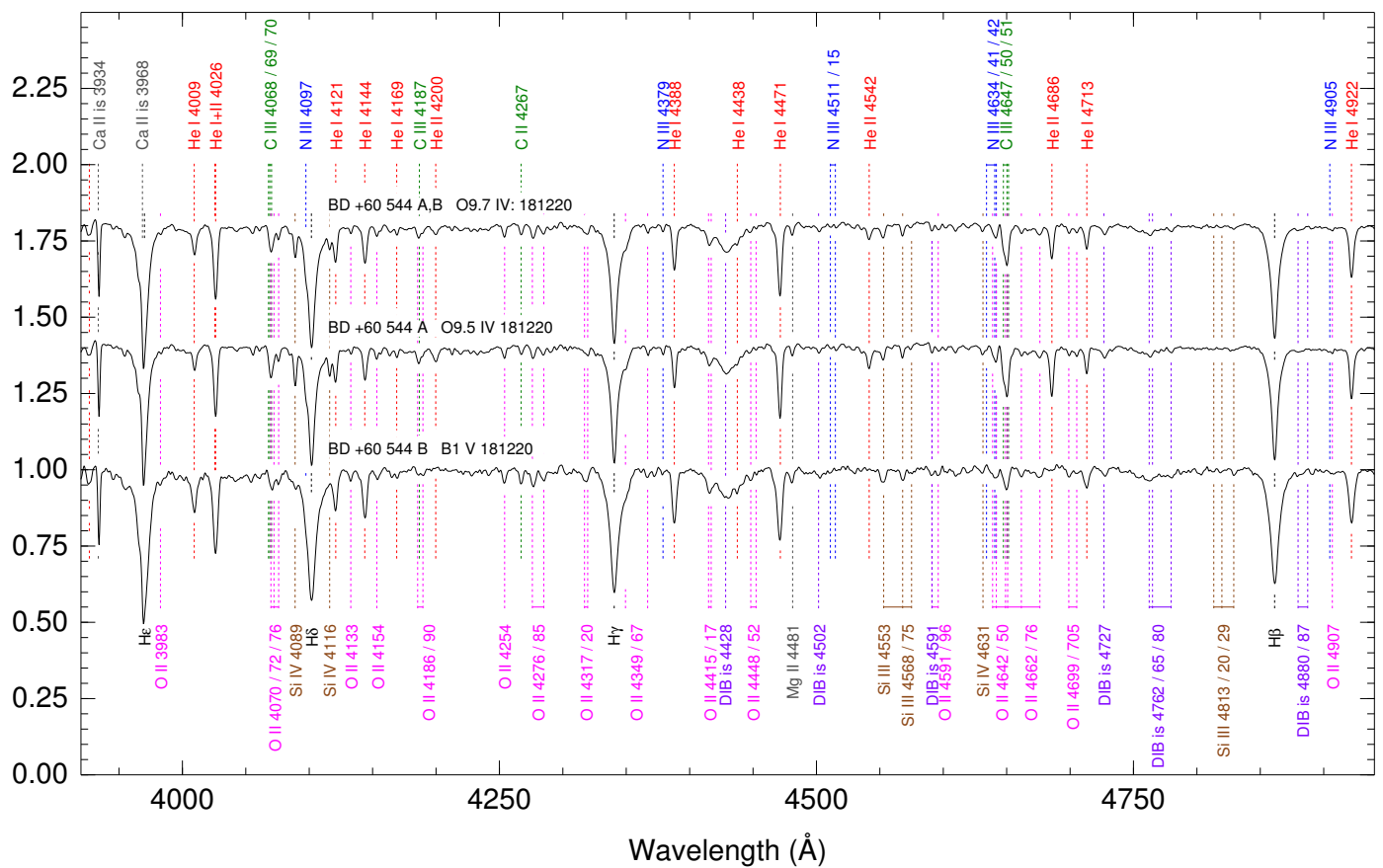


Fig. 12. Rectified spectrograms for BD +60 544 at the GOSSS spectral resolution of $R \sim 2500$ and on the stellar reference frame. For each spectrogram, the name, spectral type, and evening date (YYMMDD) are shown. The top spectrogram is the weighted combination of the two components for the 181220 epoch. Main atomic and ISM lines are indicated.

O8 V and the B component a spectral type of O9: Ve. The system has one of the smallest separations in this paper ($0''.32$); its magnitude difference is 0.7 mag. Those classifications were done with regular long-slit spectroscopy and a reanalysis of the previous data has revealed that we erroneously identified the two components by reversing the position of the slit: the one with the Oe spectrum is actually A, not B. HD 17 520 A,B has a single entry in *Gaia* DR2 but with a bad RUWE and a negative parallax. The C component, on the other hand, has a valid RUWE and we can use it to estimate the distance (assuming it is physically associated to A,B) with the same parallax zero point and prior as before to obtain $2.69^{+0.32}_{-0.26}$ kpc. HD 17 520 is in IC 1848, whose characteristics derived from *Gaia* data will be analyzed in more detail in a subsequent paper of our Villafranca series of Galactic groups with OB stars (Maíz Apellániz et al., accepted in A&A).

Despite the small magnitude difference, we are able to cleanly separate the two components with lucky spectroscopy (Fig. 13), as evidenced by the opposite behavior of $H\beta$ in A and B. The A component has a spectral classification of O9.2 Ve and the B component one of O8 Vz. The new classifications are similar to the previous GOSSS ones but with the A and B components exchanged and significantly cleaner at the same time. The merged spectrum is classified as O8.5 V with a p suffix to indicate discrepancies between weak lines caused by the composite nature. The double-peaked emission profile in $H\beta$ characteristic of high-inclination Oe/Be stars is strong in A, absent in B, and weak in merged spectrum.

There are 16 LiLiMaRlin epochs of HD 17 520 A,B and the most notorious feature is that the double-peaked emission in $H\beta$ and the even stronger one in $H\alpha$ experience not only the flux changes typical in Oe/Be stars but also large velocity variations with a peak-to-peak amplitude of ~ 200 km/s. This indicates that the A component is an SB1 and explains why it is brighter than B despite being of a later subtype. We plan to obtain additional lucky spectroscopy epochs to attempt catching A at a more favorable velocity separation and possibly identify the missing spectroscopic component.

We have two lucky imaging epochs for this system, one of them already reported in Maíz Apellániz (2010). The combination of our results and the historical WDS data indicates a small counterclockwise and outward motion of B with respect to A. The corresponding period would be of several thousands of years.

3.14. HD 24 431 A,B, a nearby isolated system

HD 24 431 was classified as O9 III in Walborn (1973) and received the same classification in GOSSS I. The WDS catalog lists a B component with $d = 0''.7$ and $\Delta m = 2.9$ mag. There is a single *Gaia* DR2 entry for this system but it has a RUWE of 1.69, likely caused by the presence of the B component. The target is isolated and we have been unable to find a stellar group associated with it in the *Gaia* DR2 data, leaving us no alternative but to use the *Gaia* DR2 parallax to estimate a distance of 812^{+61}_{-53} pc, where the uncertainty is likely an underestimation due

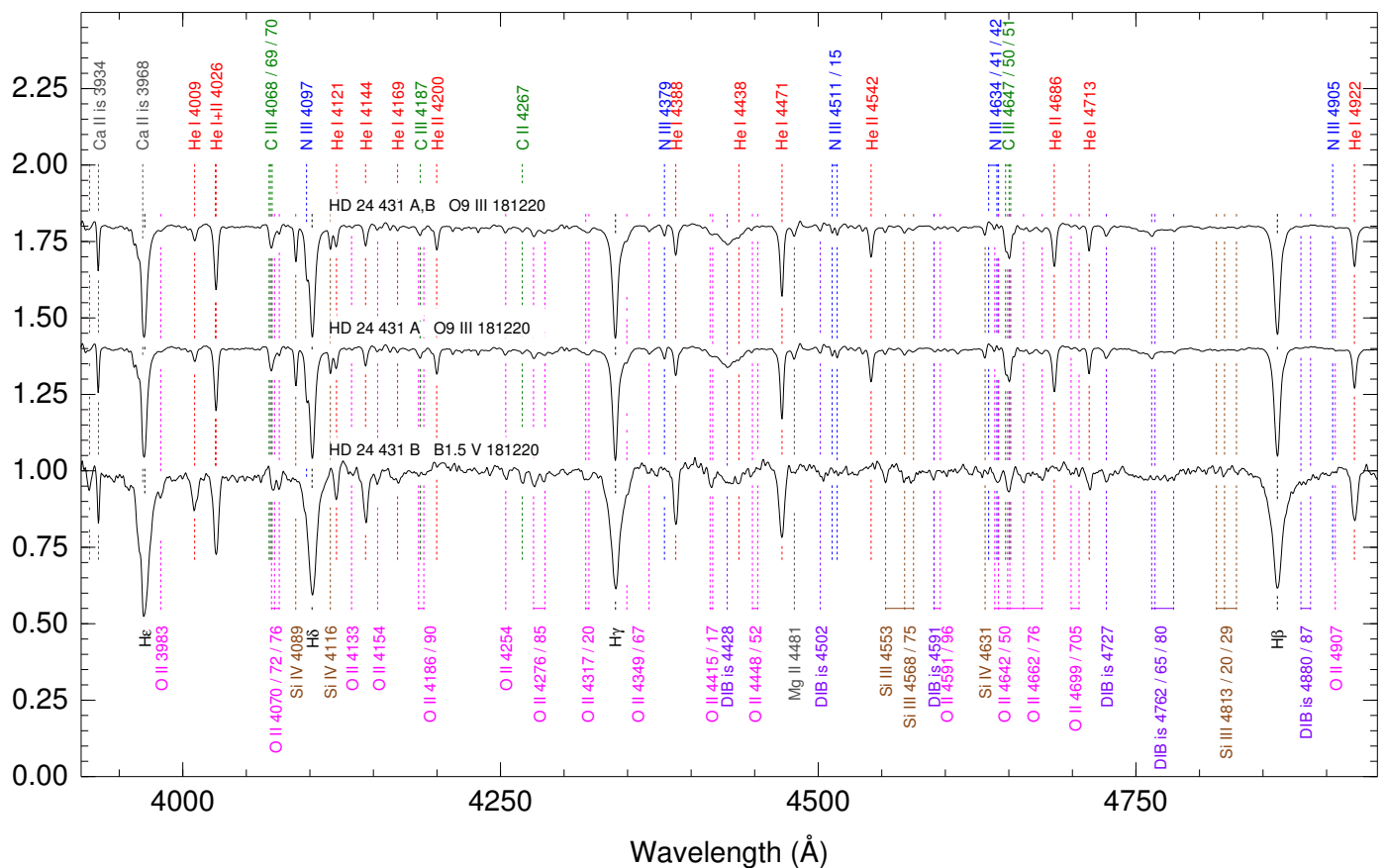


Fig. 14. Rectified spectrograms for HD 24431 at the GOSSS spectral resolution of $R \sim 2500$ and on the stellar reference frame. For each spectrogram, the name, spectral type, and evening date (YYMMDD) are shown. The top spectrogram is the weighted combination of the two components for the 181220 epoch. Main atomic and ISM lines are indicated.

Table 5. *Gaia* DR2 astrometric data for four components of the HD 164492 system with compatible parallaxes and proper motions and their aggregate results. The aggregate results use external uncertainties and include the spatial covariance terms of Lindegren et al. (2018).

comp.	ϖ (mas)	$\mu_{\alpha*}$ (mas/a)	μ_{δ} (mas/a)
A	0.6376 ± 0.0873	0.426 ± 0.122	-1.765 ± 0.097
B	0.7780 ± 0.0757	0.308 ± 0.106	-1.196 ± 0.083
D	0.8049 ± 0.1071	1.055 ± 0.140	-2.858 ± 0.112
E	0.8793 ± 0.0685	0.842 ± 0.093	-1.548 ± 0.073
	0.7841 ± 0.0613	0.630 ± 0.084	-1.706 ± 0.082

being significantly obscured by differential extinction and/or being much farther away than the rest of the stars. The first option is excluded by the 2MASS colors and the second one by the *Gaia* DR2 parallaxes (see below).

To estimate the distance to HD 164492 we follow a strategy similar to the one we used for 6 Cas, combining *Gaia* DR2 entries with good RUWE and similar parallaxes and proper motions, but selecting among the bright named WDS components. We exclude C due to its large RUWE (see above for its multiplicity, the likely culprit) and we keep the other four bright components (Table 5). Applying the same parallax zero point and prior as before we obtain a distance of $1.29^{+0.12}_{-0.10}$ kpc. We note that the proper motions indicate the presence of significant internal motions, as expected for a high-order multiple system such as this one.

We placed the slit along the A-B direction and easily separated the two components with lucky spectroscopy (Fig. 15), as expected given the large separation ($6''.26$). The A and the merged A,B spectra receive the same spectral classification as in GOSSS II (the B component is too weak to make a significant dent in the merged spectrum). The B component is a B2 Vnn star, that is, not an A supergiant but instead a mid-B star with a very large $v \sin i$ that makes it a peculiar object but not for the reason given by Gahm et al. (1983). Our spectral classification for HD 164492 B suggests possible explanations for the previous A supergiant classification: the object could be a PMS star that was observed by Gahm et al. (1983) while it was undergoing a shell phase or it could be a Be star currently in a phase with a weak disk. We also observed the C component with standard long-slit spectroscopy and assign it a spectral classification of B1 V, which must be dominated by the C2 component of Wade et al. (2017), as the C1 component is easily hidden by its large $v \sin i$ and the C3 component is significantly fainter.

There are 12 epochs of HD 164492 A in LiLiMaRlin spanning 13 years. No changes in the spectral appearance or in velocity can be appreciated in the data. There is also one FEROS epoch of HD 164492 B (possible given the large separation) that is consistent with our lucky spectroscopy observation. We have used that epoch to measure the $v \sin i$ of that fast rotator as we did for α Sco B (which has a quite similar spectrum), in this case using five He I lines: He I $\lambda 4387$, He I $\lambda 4471$, He I $\lambda 4713$, He I $\lambda 5876$, and He I $\lambda 6678$. We obtain a value of 355 ± 55 km/s. Finally, there are also 20 epochs of HD 164492 C in LiLiMaRlin

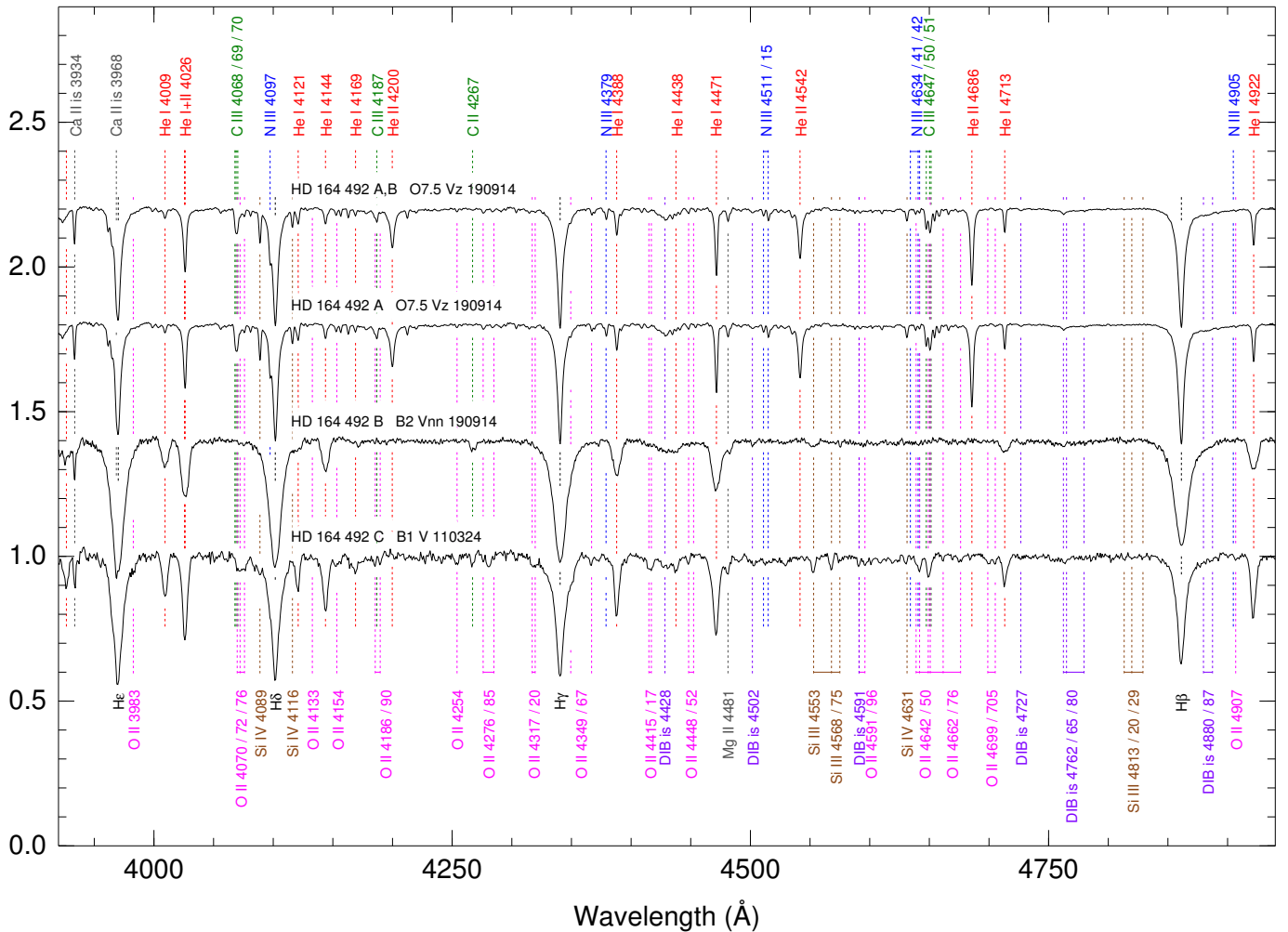


Fig. 15. Rectified spectrograms for HD 164 492 at the GOSSS spectral resolution of $R \sim 2500$ and on the stellar reference frame. For each spectrogram, the name, spectral type, and evening date (YYMMDD) are shown. The 110324 data were obtained with the 2.5 duPont telescope at LCO i.e. not with lucky spectroscopy. The top spectrogram is the weighted combination of the two components for the 190914 epoch. Main atomic and ISM lines are indicated.

spanning 6 years that show the complex line profiles produced by the SB3 system.

We have a single lucky imaging epoch for HD 164 492. In this case we list in Table 3 the measurements for three of the pairs. We did not attempt to resolve A into Aa+Ab, as the predicted separation is too small for AstraLux. Our data for the A,B and A,C pairs agree reasonably well with the *Gaia* DR2 results. For the A,H pair our magnitude difference is compatible with that of Turner et al. (2008), obtained at similar wavelengths, but is significantly larger than the NIR values of Sana et al. (2014), indicating that H is a redder object than A.

3.16. HD 168 021 A,B,C, a triple system of early-B supergiants

This system is a hierarchical triple composed of a close pair (A,B) separated by $0''.48$ and with a Δm of 1.0 mag and a more distant companion (C) $17''.2$ away and with a magnitude intermediate between those of A and B, according to the WDS catalog. Morgan et al. (1953) classified the unresolved A,B pair as B0 Ib. The C component has no precise spectral classification in the literature. There is a single *Gaia* DR2 entry for the A,B pair but it has a bad RUWE, so we cannot use it to estimate the distance to

the system. HD 168 021 C, on the other hand, has an entry with a good RUWE that allows us to obtain a value of $1.62^{+0.18}_{-0.14}$ kpc.

We spatially resolve A and B with lucky spectroscopy (Fig. 16) and we find that both are relatively similar early-B supergiants. The A component is earlier and more luminous at B0 Ia while the B component is later and less luminous at B0.2 II. The combined spectrum is classified as B0 Iab, i.e. the same spectral subtype as the Morgan et al. (1953) classification but changing the luminosity class from Ib to Iab. We also observed the C component with the WHT using regular long-slit spectroscopy and determined a spectral classification of B0.5 II. Therefore, HD 168 021 includes three similar early-type B supergiants.

3.17. HD 193 443 A,B, comparing STIS and lucky spectroscopy

HD 193 443 is a visual double separated by $0''.138$ and with a small magnitude difference (B is actually slightly brighter than A) that was studied in STIS I. In that paper spectral classifications of O8.5 III((f)) and O9.2 IV for A and B, respectively. One of the components is a spectroscopic binary (Mahy et al. 2013) and in STIS I we favored that it is B but stated that more obser-

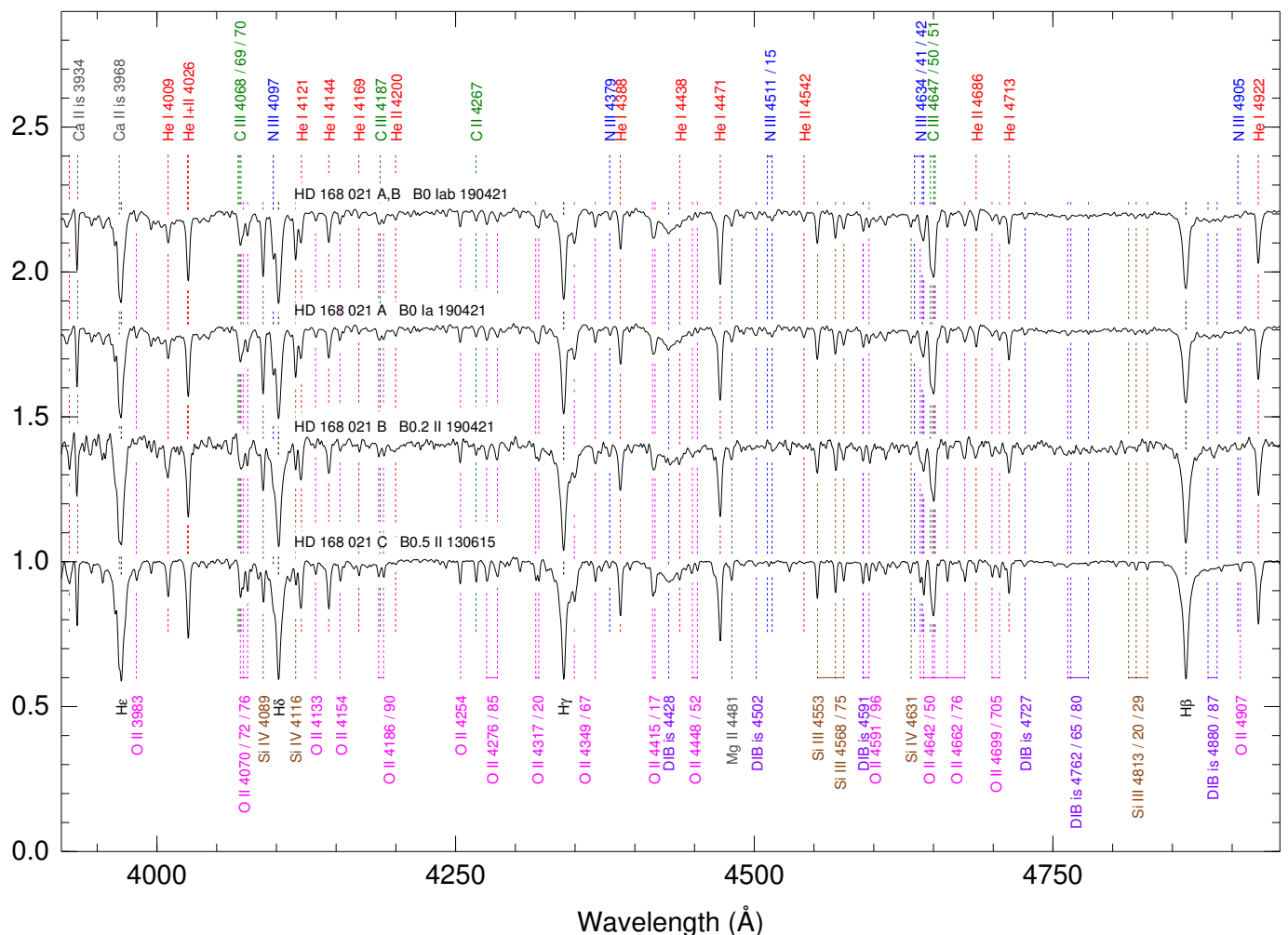


Fig. 16. Rectified spectrograms for HD 168 021 at the GOSSS spectral resolution of $R \sim 2500$ and on the stellar reference frame. For each spectrogram, the name, spectral type, and evening date (YYMMDD) are shown. The 130615 data were obtained with WHT but not with lucky spectroscopy. The top spectrogram is the weighted combination of the two components for the 190421 epoch. Main atomic and ISM lines are indicated.

variations are needed to confirm that hypothesis. There is a single entry in *Gaia* DR2 for HD 193 443 A,B but we cannot use it for a distance determination given its bad RUWE. The WDS catalog lists a C component $9''.1$ away but its RUWE is also bad. Therefore, the only way to give a *Gaia* DR2 distance to the system is by its inclusion in the Cyg OB1 association, for which Ward et al. (2020) give a value of 1.64 ± 0.24 kpc. We note that Simbad currently assigns a spectral classification of O9.5 V to HD 193 443 C and cite Mahy et al. (2015). This is a case of mistaken identity in Simbad, as that paper is referring to the spectroscopic binary, not to a visual companion. The C component is too faint to be an O star at the same distance as the A,B pair.

Among the sample in STIS I, HD 193 443 A,B is one of the two easiest systems to separate with HST (see Fig. 4 in that paper). For that reason, we attempted to separate the pair with lucky spectroscopy and we were able to do so on an occasion with exceptional seeing (we also attempted to separate the other “easy” STIS system, HD 16 429 Aa,Ab but we were unsuccessful). We compare in Fig. 17 the spectra from both setups. The spectra for each component are compatible but the lucky spectroscopy results are much noisier, illustrating the different spatial resolving power of HST and lucky spectroscopy. This translates into uncertain spectral types derived from the ground-based data.

We have 29 LiLiMaRlin epochs of HD 193 443 A,B, where there is a clear signal of the spectroscopic motion of different components. However, as already mentioned in STIS I, this is an SB3 with a static component (likely A) and two objects (likely two stars in B) moving in a spectroscopic orbit with a period of 7.467 d and a relatively low velocity amplitude ($K_1 + K_2 \sim 130$ km/s, Mahy et al. 2013) which is not large enough to make the three components appear separated at any point of the orbit. In future papers we will analyse this system in more detail with the help of new data.

3.18. HD 194 649 A,B, identifying the SB2 in a visual binary

This system was included in MONOS I, where we presented spatially unresolved spectroscopy and lucky imaging results. It is a pair with $\Delta m = 0.95$ mag (with a possible color term) and $d = 0''.40$. Similarly to HD 193 443, it includes a spectroscopic binary with a 3.392 94 d period (Mahy et al. 2013) but previous results were not able to spatially separate the A and B visual components. In MONOS I we derived spectral classifications of O6 V((f)) + O9.7: V with GOSSS data and of O6 IV((f)) + O9.5 V((f)) with LiLiMaRlin data but we acknowledged the existence of three stars contributing to the spectra and,

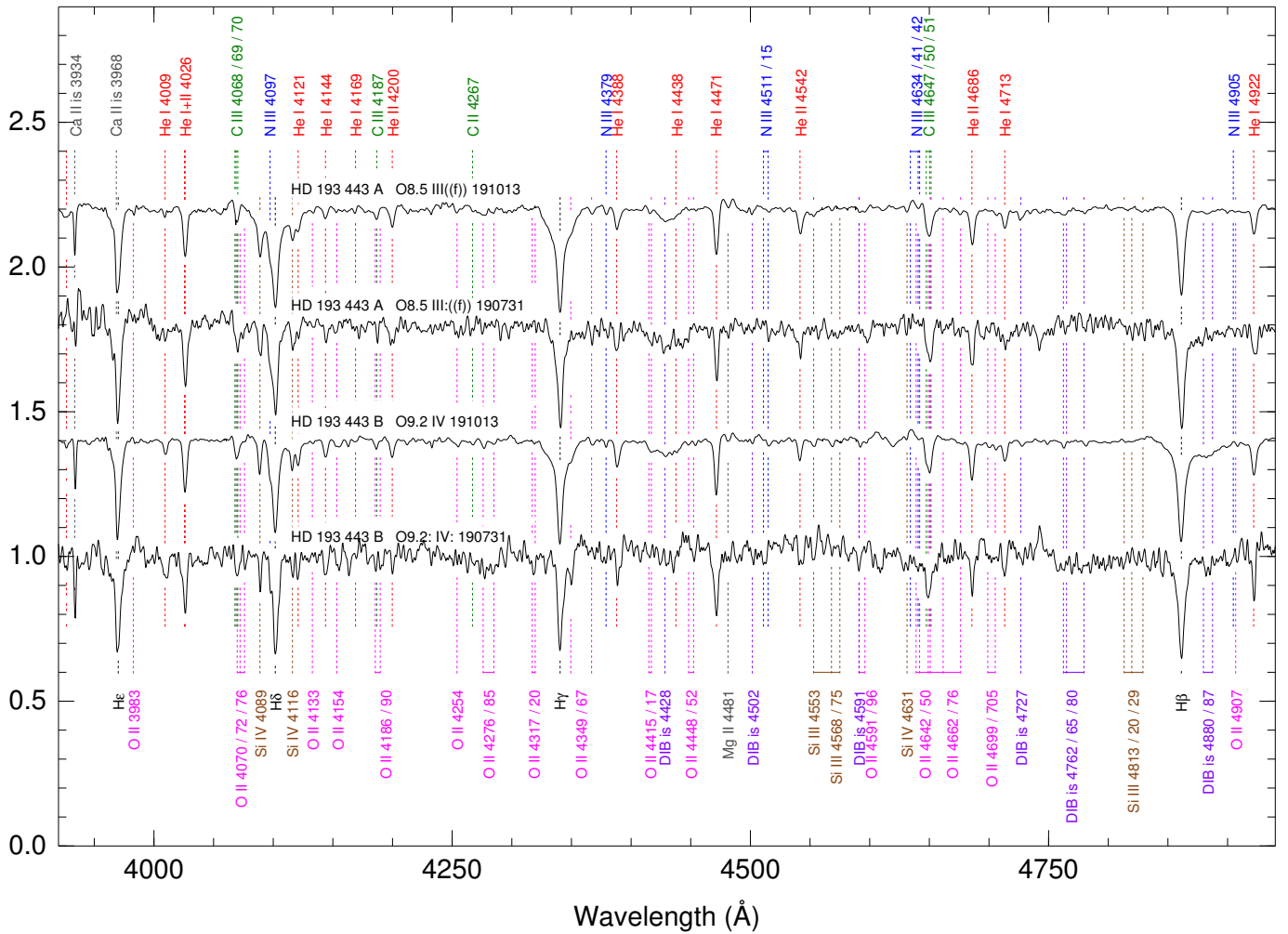


Fig. 17. Rectified spectrograms for HD 193 443 at the GOSSS spectral resolution of $R \sim 2500$ and on the stellar reference frame. For each spectrogram, the name, spectral type, and evening date (YYMMDD) are shown. The 191013 data were obtained with STIS@HST and the 190731 with WHT using lucky spectroscopy. Main atomic and ISM lines are indicated.

hence, the need for further studies of the system. HD 194 649 has a single entry in *Gaia* DR2 but without parallax or proper motions due to the extremely high RUWE of the solution, 108.1, caused by the lack of resolution of the system into its two visual components. The system is the brightest object of a little studied stellar cluster listed in Simbad as [KPS2012] MWSC 3335 (Kharchenko et al. 2013). We have searched *Gaia* DR2 to select the brightest members with good RUWE according to their proper motions and calculate the distance to the cluster (Table 6), obtaining a result of $1.62^{+0.12}_{-0.10}$ kpc.

The two visual components in HD 194 649 are clearly resolved with lucky spectroscopy (Fig. 18). The SB2 in the system is the A component, with a spectral classification of O5.5 V((f)) + O9.5 V. The B component, on the other hand, is classified as O7 Vz. The merged spectrum appears as O6 V((f)) + O9.7: V, the same classification we obtained with GOSSS data in MONOS I. These results paint a coherent picture in which the late-O star (the one with the largest velocity amplitude in the SB2) is separated in velocity in the merged spectrum near quadrature (when the lucky spectra were obtained) but the two mid-O stars (one in A and one in B) are merged into a single component in velocity. The spectral type of the primary in the merged data (O6) is an intermediate one between the two real types (O5.5 and O7). At the same time, the velocity ampli-

Table 6. *Gaia* DR2 astrometric data for 9 components of the [KPS2012] MWSC 3335 cluster (not including HD 194 649 A,B, for which no *Gaia* DR2 parallax or proper motions are available) with compatible parallaxes and proper motions and their aggregate results. The aggregate results use external uncertainties and include the spatial covariance terms of Lindegren et al. (2018).

<i>Gaia</i> DR2 ID	ϖ (mas)	μ_{α^*} (mas/a)	μ_{δ} (mas/a)
2 067 482 773 947 102 208	0.6009±0.0269	-3.140±0.045	-4.242±0.041
2 067 483 044 525 974 784	0.6250±0.0308	-3.211±0.053	-4.134±0.045
2 067 482 602 148 428 288	0.5542±0.0264	-3.166±0.043	-4.118±0.043
2 067 482 705 227 636 480	0.5593±0.0240	-3.142±0.039	-4.180±0.036
2 067 482 945 745 805 312	0.5753±0.0168	-3.300±0.027	-4.409±0.029
2 067 482 735 291 629 056	0.6065±0.0245	-3.445±0.034	-3.811±0.048
2 067 482 877 026 323 712	0.5757±0.0189	-2.890±0.035	-4.450±0.029
2 067 482 670 867 892 352	0.5944±0.0194	-3.254±0.035	-4.293±0.029
2 067 482 945 745 805 440	0.5826±0.0230	-3.040±0.039	-4.181±0.034
	0.5852±0.0413	-3.177±0.065	-4.036±0.065

tude of the primary in the SB2 in the merged data is lower than the real value: if we measure the velocity difference between the two components in the merged data we obtain ~ 275 km/s but if we do it in the separated spectrum we get ~ 325 km/s (at $R \sim 2500$ resolution, individual uncertainties for components

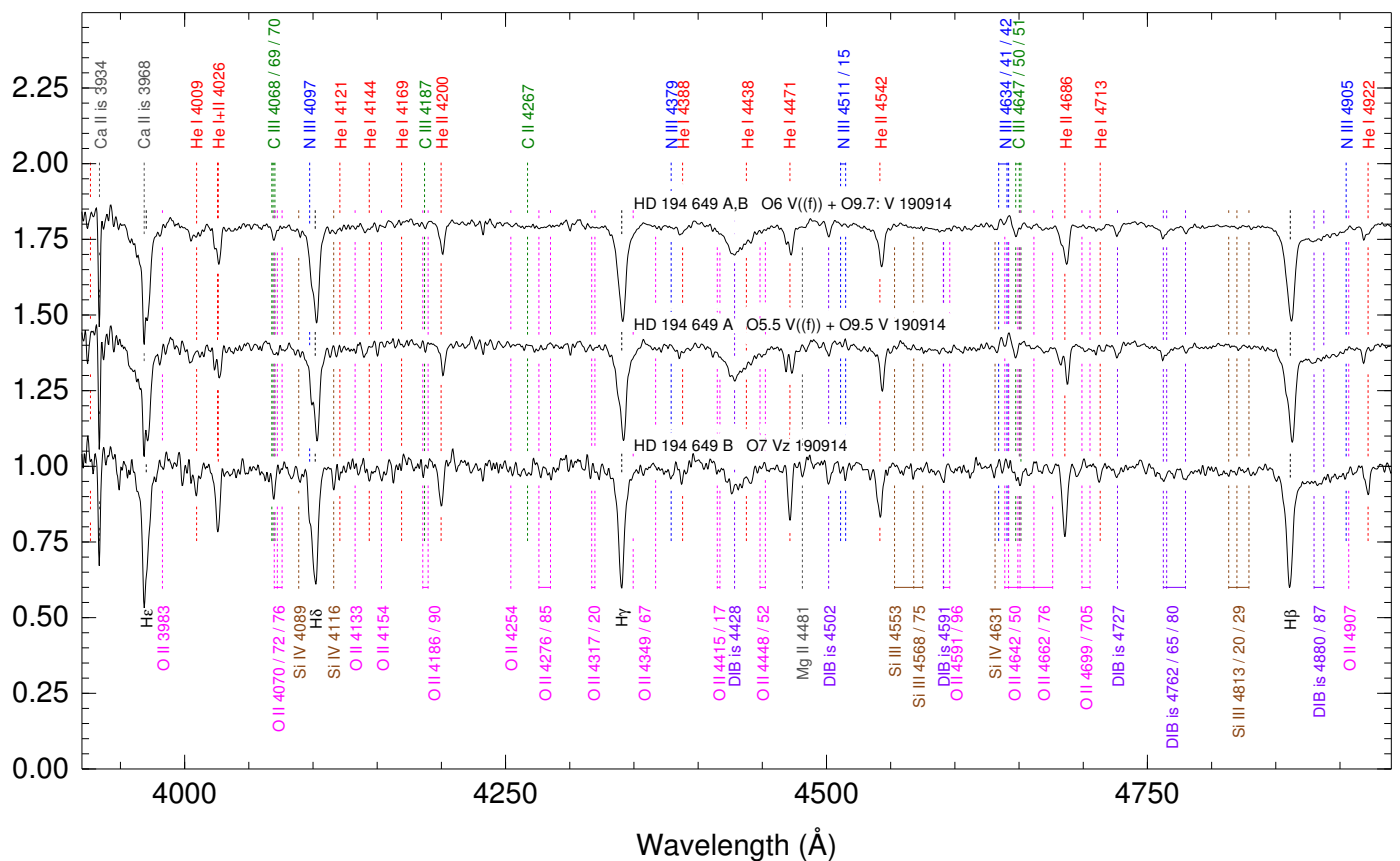


Fig. 18. Rectified spectrograms for HD 194 649 at the GOSSS spectral resolution of $R \sim 2500$ and on the heliocentric reference frame. For each spectrogram, the name, spectral type, and evening date (YYMMDD) are shown. The top spectrogram is the weighted combination of the two components for the 190914 epoch. Main atomic and ISM lines are indicated.

well resolved in velocity are 10-15 km/s). According to Mahy et al. (2013), $K_1 = 76.3$ km/s and $K_2 = 192.1$ km/s with a circular orbit, which agrees reasonably well with our measurement in the merged spectrum. However, that means that the true value for K_1 is likely to be closer to 125 km/s. The importance of that result is that it changes the mass ratio from ~ 2.5 to ~ 1.5 . The first value is hard to reconcile with what one expects for an O6 V and an O9.5 V stars but the second value is a reasonable one for an O5.5 V and an O9.5 V stars. In the future we plan to obtain further data and derive a new orbit within the MONOS project. Finally, the measured 0.95 mag difference between A and B is consistent with the expected value for the derived spectral classifications.

3.19. HD 191 201 A,B, another visual binary with an SB2 component

This system was included in MONOS I, where we presented spatially unresolved spectroscopy and lucky imaging results. It is a pair with $\Delta m = 1.8$ mag and $d = 0''.98$. Similarly to HD 194 649, it includes a spectroscopic binary with an 8.333 832 d period (Stickland & Lloyd 2001) and for this system it is clear that it resides in the A component. In GOSSS I we classified the A component as O9.5 III + B0 IV and the B component as O9.7 III. HD 191 201 A,B has a single entry in *Gaia* DR2 but with a bad RUWE that does not allow us to use its astrometry to calculate a distance. The WDS catalog lists a C component for

this multiple system that does have good-quality astrometry in *Gaia* DR2. We use it to derive a distance of $2.02^{+0.13}_{-0.11}$ kpc.

We easily resolve the two components of HD 191 201 with lucky spectroscopy (Fig. 19). The spectral classification for A is O9.5 III + B0 V, identical to that of GOSSS I except for the lower luminosity class of the spectroscopic secondary. The spectral classification for B is O9.7 V, downgraded in luminosity class from III with respect to GOSSS I. The difference is likely caused by the lower contamination in the lucky spectroscopy data compared to the regular long-slit spectroscopy used in the original paper but there are two additional factors to consider. The first one is that since GOSSS I we have decided to give more weight to the Si/He criterion for the luminosity classification of late-type O stars in detriment of the He/He criterion, as the former criterion is less sensitive to the effect of hidden binaries. The second one is that HD 191 201 B appears to be an object with a very low $v \sin i$. In any case, the change in luminosity classification yields a much better agreement between the expected and the measured Δm between A and B. The spectral classification for the merged spectrum is O9.5 III + O9.7 V and we see a similar effect as the one described for HD 194 649: the velocity difference between the two spectroscopic components is larger in the separated spectrum (~ 300 km/s, obtained near quadrature) than in the merged spectrum (~ 225 km/s). HD 191 201 will also be studied in an incoming MONOS paper using LiLiMaRlin data.

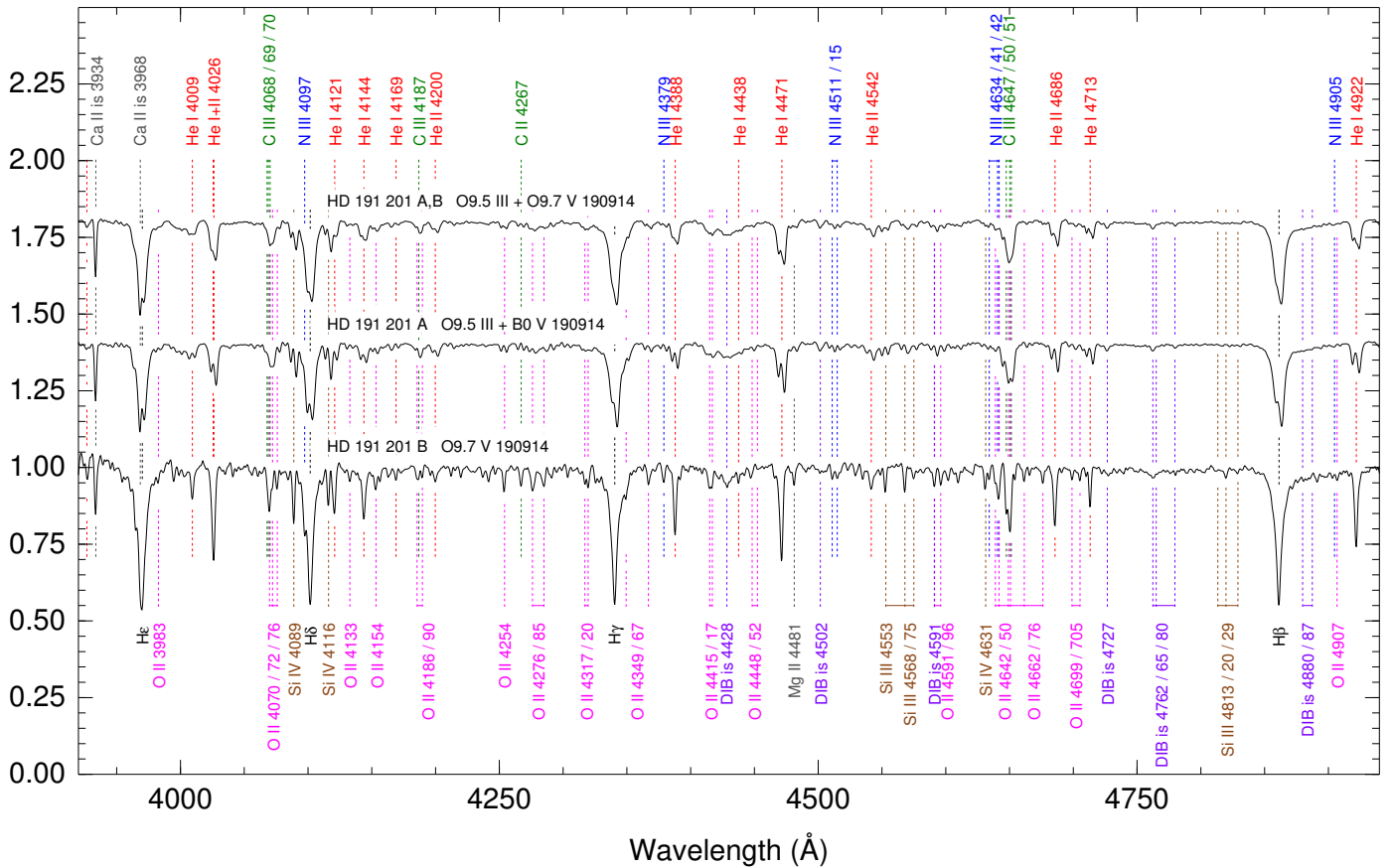


Fig. 19. Rectified spectrograms for HD 191 201 at the GOSSS spectral resolution of $R \sim 2500$ and on the heliocentric reference frame. For each spectrogram, the name, spectral type, and evening date (YYMMDD) are shown. The top spectrogram is the weighted combination of the two components for the 190914 epoch. Main atomic and ISM lines are indicated.

4. Summary and future work

In this paper we present spatially resolved intermediate-resolution blue-violet spectroscopy of 19 massive close binaries. The combined sample of LS I and this paper contains 23 systems with angular separations between $0''.138$ and $6''.19$ and physical plane-of-the-sky separations between 100 AU and 8000 AU. The most relevant results are:

- For two stars (FN CMa B and 6 Cas B) that had been previously identified as O stars based on spatially unresolved data, we obtain for the first time spatially disentangled spectra and derive accurate spectral classifications. In both cases the companion is a more evolved, visually brighter supergiant, of B type in the first case and of A type in the second one. We note that 6 Cas is the only known Galactic case of an A supergiant + O binary.
- We determine that two companions to massive stars (α Sco B and HD 164 492 B) are fast rotators of B2 spectral type. In both cases the large $v \sin i$ likely contributed to their misidentification in the literature, in the first case as a B star of a later subtype and in the second one as an A supergiant. We also note the tendency, already noticed in LS I and mentioned for some further cases in STIS I, of the visual companions of massive stars to be fast rotators of B spectral type.
- We have extended the technique of lucky spectroscopy to include three systems (α Sco A,B, CS Cam A,B, and HD 164 492 A,B) with extreme brightness differences (more than 3.5 mag).
- Using data from an occasion with exceptional seeing, we have been able to spatially separate HD 193 443 A,B, a very close system ($d = 0''.138$) that we had also successfully separated with STIS. The resulting spectra, however, are significantly noisier than the STIS equivalents, indicating that we have reached the limit of the possibilities of lucky spectroscopy (at least with our current setup) for objects with small magnitude differences.
- We have extended the range of the technique to objects much fainter than those in LS I (down to primaries with $B = 11$ mag). We have been able to do so in part due to the use of a different CCD that has a better duty cycle that allows us to stay on target 98% of the time as opposed to just 7%.
- In LS I the stars had relatively similar spectral types (mid-O to early-B). Here we have expanded the technique to demonstrate that it works with primaries of other spectral types and with systems that differ greatly between primary and secondary. In this way we have observed as primaries an A supergiant (6 Cas A), a WR star (HD 219 460 B = WR 157), and an M supergiant (α Sco A). The secondaries in those cases are late-O to early-B stars.
- Three of the objects in our sample have surprising identities. HD 51 756 B and BD +60 544 are two bright stars identified as O-type for the first time and HD 8768 A is a new member of the rare OC category. In the three cases the identification has been possible thanks to the elimination of the contamination from a nearby companion with lucky spectroscopy.

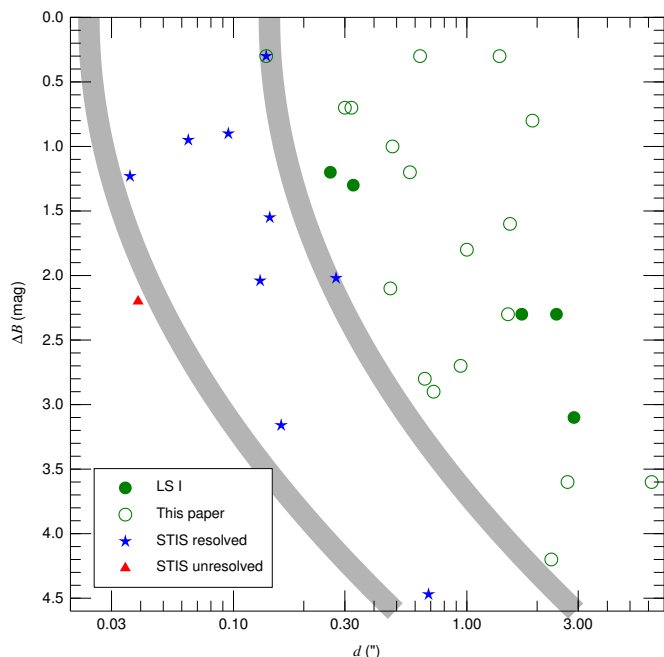


Fig. 20. Binary systems resolved using lucky spectroscopy with WHT/ISIS (in LS I and here) and HST/STIS and unresolved systems using HST/STIS in the $d - \Delta B$ (separation- B magnitude difference) plane. The gray curves mark the tentative empirical boundaries between the regions in the plane accessible with different techniques: the left one is for HST/STIS and the right one for lucky spectroscopy with WHT/ISIS. This is an updated version of Fig. 4 in STIS I.

- For four of the visual systems in which one of the components is an SB2 (σ Ori, HD 219 460, HD 194 649, and HD 191 201) we identify the doubled-lined components and provide the spectral classifications. For HD 219 460 A it is the first time the SB2 nature is noted and for HD 194 649 we identify the A component as the SB2 for the first time. For another seven systems (FN CMa, σ Sco, HD 51 756, HD 218 195, HD 17 520, HD 24 431, and HD 164 492) we detect signs of spectroscopic binarity in the LiLiMaRlin data.

We plot in Figure 20 the magnitude difference as a function of separation for the systems in LS I, STIS I, and this paper. The boundaries for the regions accessible for the two methods are just empirical approximations based on the existing data. In particular, the capabilities of lucky spectroscopy depend on the seeing at the moment of the observation and a star that is not spatially resolved today may be resolved tomorrow with the same setup. Also, objects near the boundary may be spatially resolved but at the cost of a lower S/N due to the noise produced by the separation process. In that way, the spectrum of σ Sco Ab in this paper is noisier than that of HD 168 021, as both have similar separations but the first one has a larger ΔB . Along a similar line, the lucky spectra for HD 193 443 A,B have been separated but at the cost of a poor S/N, as the system lies at the limit of what can be done with lucky spectroscopy and the observation took place with exceptional seeing (the spectra were easily separated with STIS with good S/N). The other object spatially resolved by STIS that lies at the limit accessible by lucky spectroscopy shown in Fig. 20 corresponds to HD 16 429 Aa,Ab. We attempted to separate that system twice with lucky spectroscopy but the conditions were not optimal and we failed.

For the future we plan to obtain additional lucky spectroscopy along different lines:

- Observe additional objects using the same configurations as in the first two papers.
- Obtain observations at higher spectral resolution to better study spectroscopic binaries in hierarchical systems.
- Extend the technique to longer wavelengths, where there are less spectral lines of interest but where lucky spectroscopy should work better and allow for the disentangling of systems with smaller separations and/or higher extinctions.
- Attempt the technique with other telescopes.

Acknowledgements. J.M.A., C.F., A.S., M.P.G., and G.H. acknowledge support from the Spanish Government Ministerio de Ciencia through grant PGC2018-95 049-B-C22. R.H.B. acknowledges support from the ESAC Faculty Visitor Program. I.N. and S.S.-D. acknowledge support from the Spanish Government Ministerio de Ciencia through grant PGC2018-93 741-B-C21/22 (MICIU/AEI/FEDER, UE). S.S.-D. also acknowledges funding from the Spanish Government Ministerio de Ciencia through grants SEV 2015-0548 and CEX2019-920-S, and from the Canarian Agency for Research, Innovation and Information Society (ACHISI), of the Canary Islands Government, and the European Regional Development Fund (ERDF), under grant with reference ProID2017010115. This paper is based on (a) lucky (and regular long-slit) spectroscopy obtained with the 4.2 m William Herschel Telescope (WHT) at the Observatorio del Roque de los Muchachos (ORM) on the island of La Palma, Spain; (b) lucky imaging obtained with the 2.2 m Telescope at the Centro Astronómico Hispano en Andalucía (CAHA) in Almería, Spain; (c) IFU spectroscopy obtained with the 2 m Liverpool Telescope (LT) at the Observatorio del Roque de los Muchachos (ORM) on the island of La Palma, Spain as part of GOSSS; (d) long-slit spectroscopy obtained with the 2.5 duPont Telescope at the Observatorio de Las Campanas (LCO) in Chile; and (e) high-resolution échelle spectroscopy from the LiLiMaRlin project obtained with a variety of spectrographs: HERMES at the 1.2 m Mercator Telescope (MT) at the Observatorio del Roque de los Muchachos (ORM) on the island of La Palma, Spain; ELODIE at the 1.93 m Observatoire de Haute-Provence (OHP) Telescope, France; FEROS at the 2.2 m Telescope of the Observatorio de La Silla in Chile; CAFÉ at the 2.2 m Centro Astronómico Hispano en Andalucía (CAHA) Telescope, Almería, Spain; FIES at the 2.5 Nordic Optical Telescope (NOT) at the Observatorio del Roque de los Muchachos (ORM) on the island of La Palma, Spain; and UVES at the 8.2 m Kueyen Telescope at the Observatorio Paranal in Chile. Some of the MT and NOT data were obtained from the IACOB spectroscopic database (Simón-Díaz et al. 2011b,a, 2015b). This paper has made use of data from the European Space Agency (ESA) mission *Gaia* (<https://www.cosmos.esa.int/gaia>), processed by the *Gaia* Data Processing and Analysis Consortium (DPAC, <https://www.cosmos.esa.int/web/gaia/dpac/consortium>). Funding for the DPAC has been provided by national institutions, in particular the institutions participating in the *Gaia* Multilateral Agreement. This paper has also made use of the Washington Double Star (WDS) catalog (Mason et al. 2001) and the Skiff (2014) catalog of spectral classifications. The authors would like to thank the personnel of the WHT, CAHA, LT, LCO, MT, La Silla, and NOT observatories for their support and hospitality throughout the years. We dedicate this paper to our deceased colleagues, Virpi S. Niemelä and Nolan R. Walborn, who they surely would have enjoyed having access to data like the ones presented here.

References

- Adams, W. S. & Joy, A. H. 1921, *PASP*, 33, 206
Arias, J. I., Walborn, N. R., Simón Díaz, S., et al. 2016, *AJ*, 152, 31
Aydin, C. 1979, *Ap&SS*, 64, 481
Beavers, W. I. & Cook, D. B. 1980, *ApJS*, 44, 489
Berlanas, S. R., Herrero, A., Comerón, F., et al. 2020, arXiv e-prints, arXiv:2008.09917
Cami, J., Sonnentrucker, P., Ehrenfreund, P., & Foing, B. H. 1997, *A&A*, 326, 822
Campillay, A. R., Arias, J. I., Barbá, R. H., et al. 2019, *MNRAS*, 484, 2137
Corbally, C. J. 1984, *ApJS*, 55, 657
Dorda, R., Negueruela, I., González-Fernández, C., & Marco, A. 2018, *A&A*, 618, A137
Finsen, W. S. 1956, Circular of the Union Observatory Johannesburg, 115, 259
Gahm, G. F., Ahlin, P., & Lindroos, K. P. 1983, *A&AS*, 51, 143
Garrison, R. F. 1967, *ApJ*, 147, 1003

- Garrison, R. F., Hiltner, W. A., & Schild, R. E. 1977, *ApJS*, 35, 111
- González, J. F., Hubrig, S., Przybilla, N., et al. 2017, *MNRAS*, 467, 437
- Hardorp, J., Rohlf, K., Slettebak, A., & Stock, J. 1959, *Hamburger Sternw. Warner & Swasey Obs.*, C01, 0
- Hiltner, W. A. 1956, *ApJS*, 2, 389
- Hiltner, W. A., Garrison, R. F., & Schild, R. E. 1969, *ApJ*, 157, 313
- Holgado, G., Simón-Díaz, S., Barbá, R. H., et al. 2018, *A&A*, 613, A65
- Holgado, G., Simón-Díaz, S., Haemmerlé, L., et al. 2020, *A&A*, 638, A157
- Johnson, H. L. & Morgan, W. W. 1953, *ApJ*, 117, 313
- Keenan, P. C. & McNeil, R. C. 1989, *ApJS*, 71, 245
- Kharchenko, N. V., Piskunov, A. E., Schilbach, E., Röser, S., & Scholz, R.-D. 2013, *A&A*, 558, A53
- Krelowski, J., Schmidt, M., & Snow, T. P. 1997, *PASP*, 109, 1135
- Law, N. M., Mackay, C. D., & Baldwin, J. E. 2006, *A&A*, 446, 739
- Lesh, J. R. 1968, *ApJS*, 17, 371
- Lindegren, L. et al. 2018, https://www.cosmos.esa.int/documents/29201/1770596/Lindegren_GaiaDR2_Astrometry_extended.pdf
- Mahy, L., Rauw, G., De Becker, M., Eenens, P., & Flores, C. A. 2013, *A&A*, 550, A27
- Mahy, L., Rauw, G., De Becker, M., Eenens, P., & Flores, C. A. 2015, *A&A*, 577, A23
- Maíz Apellániz, J. 2001, *AJ*, 121, 2737
- Maíz Apellániz, J. 2005, in *ESA Special Publication*, Vol. 576, *The Three-Dimensional Universe with Gaia*, ed. C. Turon, K. S. O’Flaherty, & M. A. C. Perryman, 179
- Maíz Apellániz, J. 2010, *A&A*, 518, A1
- Maíz Apellániz, J. 2015, *MmSAI*, 86, 553
- Maíz Apellániz, J. 2019, *A&A*, 630, A119
- Maíz Apellániz, J., Alfaro, E. J., & Sota, A. 2008, *arXiv:0804.2553*
- Maíz Apellániz, J. & Barbá, R. H. 2018, *A&A*, 613, A9
- Maíz Apellániz, J. & Barbá, R. H. 2020, *A&A*, 636, A28 (STIS I)
- Maíz Apellániz, J., Barbá, R. H., Simón-Díaz, S., et al. 2018, *A&A*, 615, A161 (LS I)
- Maíz Apellániz, J., Sota, A., Arias, J. I., et al. 2016, *ApJS*, 224, 4 (GOSSS III)
- Maíz Apellániz, J., Sota, A., Walborn, N. R., et al. 2011, in *HSA* 6, 467–472
- Maíz Apellániz, J., Trigueros Páez, E., Jiménez Martínez, I., et al. 2019a, in *HSA* 10, 420 (LiLiMaRlin)
- Maíz Apellániz, J., Trigueros Páez, E., Negueruela, I., et al. 2019b, *A&A*, 626, A20 (MONOS I)
- Mason, B. D., Gies, D. R., Hartkopf, W. I., et al. 1998, *AJ*, 115, 821
- Mason, B. D., Wycoff, G. L., Hartkopf, W. I., Douglass, G. G., & Worley, C. E. 2001, *AJ*, 122, 3466
- Morgan, W. W., Code, A. D., & Whitford, A. E. 1955, *ApJS*, 2, 41
- Morgan, W. W. & Keenan, P. C. 1973, *ARA&A*, 11, 29
- Morgan, W. W. & Roman, N. G. 1950, *ApJ*, 112, 362
- Morgan, W. W., Whitford, A. E., & Code, A. D. 1953, *ApJ*, 118, 318
- North, J. R., Davis, J., Tuthill, P. G., Tango, W. J., & Robertson, J. G. 2007, *MNRAS*, 380, 1276
- Pantaleoni González, M., Maíz Apellániz, J., Barbá, R. H., & Negueruela, I. 2020, *RNAAS*, 4, 12
- Reimers, D., Hagen, H.-J., Baade, R., & Braun, K. 2008, *A&A*, 491, 229
- Rivinius, T., Stahl, O., Štefl, S., et al. 2011, in *IAUS*, Vol. 272, 543–544
- Roman-Lopes, A., Román-Zúñiga, C., Tapia, M., et al. 2018, *ApJ*, 855, 68
- Rydstrom, B. A. 1978, *A&AS*, 32, 25
- Sana, H., Le Bouquin, J.-B., Lacour, S., et al. 2014, *ApJS*, 215, 15
- Simón-Díaz, S., Caballero, J. A., Lorenzo, J., et al. 2015a, *ApJ*, 799, 169
- Simón-Díaz, S., Castro, N., García, M., & Herrero, A. 2011a, in *IAUS*, Vol. 272, 310–312
- Simón-Díaz, S., Garcia, M., Herrero, A., Maíz Apellániz, J., & Negueruela, I. 2011b, in *Stellar Clusters & Associations: A RIA Workshop on Gaia*, 255–259
- Simón-Díaz, S., Godart, M., Castro, N., et al. 2017, *A&A*, 597, A22
- Simón-Díaz, S. & Herrero, A. 2014, *A&A*, 562, A135
- Simón-Díaz, S., Herrero, A., Sabín-Sanjulián, C., et al. 2014, *A&A*, 570, L6
- Simón-Díaz, S., Negueruela, I., Maíz Apellániz, J., et al. 2015b, in *HSA* 8, 576–581
- Skiff, B. A. 2014, *VizieR Online Data Catalog*, B/mk
- Smith, L. F., Shara, M. M., & Moffat, A. F. J. 1996, *MNRAS*, 281, 163
- Sota, A., Maíz Apellániz, J., Morrell, N. I., et al. 2014, *ApJS*, 211, 10 (GOSSS II)
- Sota, A., Maíz Apellániz, J., Walborn, N. R., et al. 2011, *ApJS*, 193, 24 (GOSSS I)
- Stickland, D. J. & Lloyd, C. 2001, *The Observatory*, 121, 1
- Stone, S. N. & Struve, O. 1954, *PASP*, 66, 191
- Swings, J. P. & Preston, G. W. 1978, *ApJ*, 220, 883
- Talavera, A. & Gómez de Castro, A. I. 1987, *A&A*, 181, 300
- Turner, D. G., Moffat, A. F. J., Lamontagne, R., & Maitzen, H. M. 1983, *AJ*, 88, 1199
- Turner, N. H., ten Brummelaar, T. A., Roberts, L. C., et al. 2008, *AJ*, 136, 554
- Wade, G. A., Shultz, M., Sikora, J., et al. 2017, *MNRAS*, 465, 2517
- Walborn, N. R. 1972, *AJ*, 77, 312
- Walborn, N. R. 1973, *AJ*, 78, 1067
- Ward, J. L., Kruijssen, J. M. D., & Rix, H.-W. 2020, *MNRAS*, 495, 663